

Flexible Models for Simple Longitudinal Data

Helen Ogden

University of Southampton, UK

Abstract

We propose a new method for modelling simple longitudinal data. We aim to do this in a flexible manner (without restrictive assumptions about the shapes of individual trajectories), while exploiting structural similarities between the trajectories. Hierarchical models (such as linear mixed models, generalised additive mixed models and hierarchical generalised additive models) are commonly used to model longitudinal data, but fail to meet one or other of these requirements: either they make restrictive assumptions about the shape of individual trajectories, or fail to exploit structural similarities between trajectories. Functional principal components analysis promises to fulfil both requirements, and methods for functional principal components analysis have been developed for longitudinal data. However, we find that existing methods sometimes give poor-quality estimates of individual trajectories, particularly when the number of observations on each individual is small. We develop a new approach, which we call hierarchical modelling with functional principal components. Inference is conducted based on the full likelihood of all unknown quantities, with a penalty term to control the balance between fit to the data and smoothness of the trajectories. We run simulation studies to demonstrate that the new method substantially improves the quality of inference relative to existing methods across a range of examples, and apply the method to data on changes in body composition in adolescent girls.

Keywords: Clustered data; Functional principal components analysis; Mixed-effects models; Penalised likelihood; Smoothing; Subject-specific inference

1 Introduction

We consider a simple longitudinal data setup, in which observations are made on each of d subjects, with observations on subject i at n_i time points. Writing Y_{ij} for the observation on subject i at time point t_{ij} , we might model

$$Y_{ij} = \mu_i(t_{ij}) + \epsilon_{ij}, \quad i = 1, \dots, d, \quad j = 1, \dots, n_i, \quad (1)$$

where $\mu_i(\cdot)$ is the trajectory for subject i (a function describing how the mean response for subject i varies over time), and $\epsilon_{ij} \sim N(0, \sigma^2)$ are independent error terms. We aim to allow flexible dependence on time in the trajectories and to exploit structural similarities between trajectories to improve estimation.

A large range of methods exist for this problem, and we review some of them in section 2. Hierarchical models (such as linear mixed models, generalised additive mixed models and hierarchical generalised additive models) are commonly used to model longitudinal data, but either make restrictive assumptions about the shape of individual trajectories or fail to exploit structural similarities between trajectories. To allow flexible dependence on time while still exploiting structural similarities between trajectories, we turn to functional principal components analysis, in which each trajectory is expressed as the population mean plus a subject-specific combination of a small number of unknown functions. These functions, the functional principal components, are chosen to be able to best explain the variation between individual trajectories. In practice, a large (or infinite) number of functional principal components may be needed to exactly express the true data generating process, but typically a very high-quality approximation may be obtained with a small number of components.

Methods for functional principal components analysis with longitudinal data (often known as sparse functional principal components analysis) have been developed previously (Yao et al., 2005; Di et al., 2009). However, we will show that these methods sometimes give poor-quality estimates of the individual trajectories, particularly when the number of observations on each individual is small.

In this paper, we develop a new approach for flexible modelling of longitudinal data, which we call hierarchical modelling with functional principal components (HM-FPC). By contrast with existing methods for sparse functional principal components analysis, we conduct inference based on the full likelihood of all unknown quantities. We include a penalty term to control the balance between fit to the data and smoothness of the trajectories.

In section 4, we run simulation studies across a range of examples to demonstrate that HM-FPC substantially improves the quality of inference relative to existing methods, in terms of estimation error (often several times smaller than existing methods) and confidence intervals (with close to correct coverage, in cases where existing methods substantially under-cover).

In section 5, we apply our hierarchical models with functional principal components to data on changes in body composition in adolescent girls.

The setup (1) is a simple one, with normal errors and a single covariate (time). We focus on this simple setup to make the methods development and coding more straightforward, and to make the main ideas easier to understand. The same general ideas have the scope to be applied to more complex modelling problems, and we discuss some possible extensions in section 6.

2 Existing modelling approaches

2.1 Hierarchical models for longitudinal data

Hierarchical models are commonly used to model longitudinal data. We will show that such models either make restrictive assumptions about the shapes of individual trajectories, or fail to exploit structural similarities in the shapes of different trajectories.

Figure 1 shows fitted trajectories for a subset of four subjects for various models, each fitted to a common simulated dataset with 100 subjects and 5 observations per subject. The data and residuals for the four chosen subjects are overlaid.

Linear mixed-effects models (LMMs) typically assume straight-line trajectories. In a random intercepts LMM (Figure 1a), each individual trajectory is found by shifting a population line up or down by a constant. A random slopes LMM (Figure 1b) also allows variation in the slope of each individual trajectory.

Generalised additive mixed models (GAMMs) (Lin and Zhang, 1999) allow trajectories to be smooth curves, but assume simple relationships between different trajectories. In a random intercept GAMM (Figure 1c), each individual trajectory is found by shifting the population trajectory up or down by a constant. A random slopes GAMM (Figure 1d) also allows variation in the slope of each individual trajectory. GAMMs do not make restrictive assumptions on the population trajectory, but still make a strong assumption that the individual trajectories are found by shifting the population trajectory up or down by a constant, or tilting the trajectory to change the slope. There is typically no reason to believe individual trajectories should be found by such a simple modification of the population trajectory.

Existing classes of hierarchical generalised additive model (HGAMs) provide full flexibility in modelling individual trajectories, but with limited information sharing between individuals. Pedersen et al. (2019) describes several classes of HGAM; the most relevant here is the HGAM-GS (Figure 1e), where the individual trajectories are allowed to be arbitrary smooth curves, shrunk towards a common population trajectory and assumed to be similarly smooth to one another. The HGAM-GS is very flexible, allowing any shape of individual trajectories, but does not share shape information between trajectories, beyond their level of smoothness. The fitted curves interpolate the data, but there is a high level of uncertainty about the true trajectory between the data points. Figure 2a shows the same fitted trajectories as in Figure 1e, separated into four plots, with 95% pointwise confidence intervals overlaid. The true trajectories used to simulate the data are overlaid as dashed curves. For the first two individuals plotted, the HGAM-GS fitted

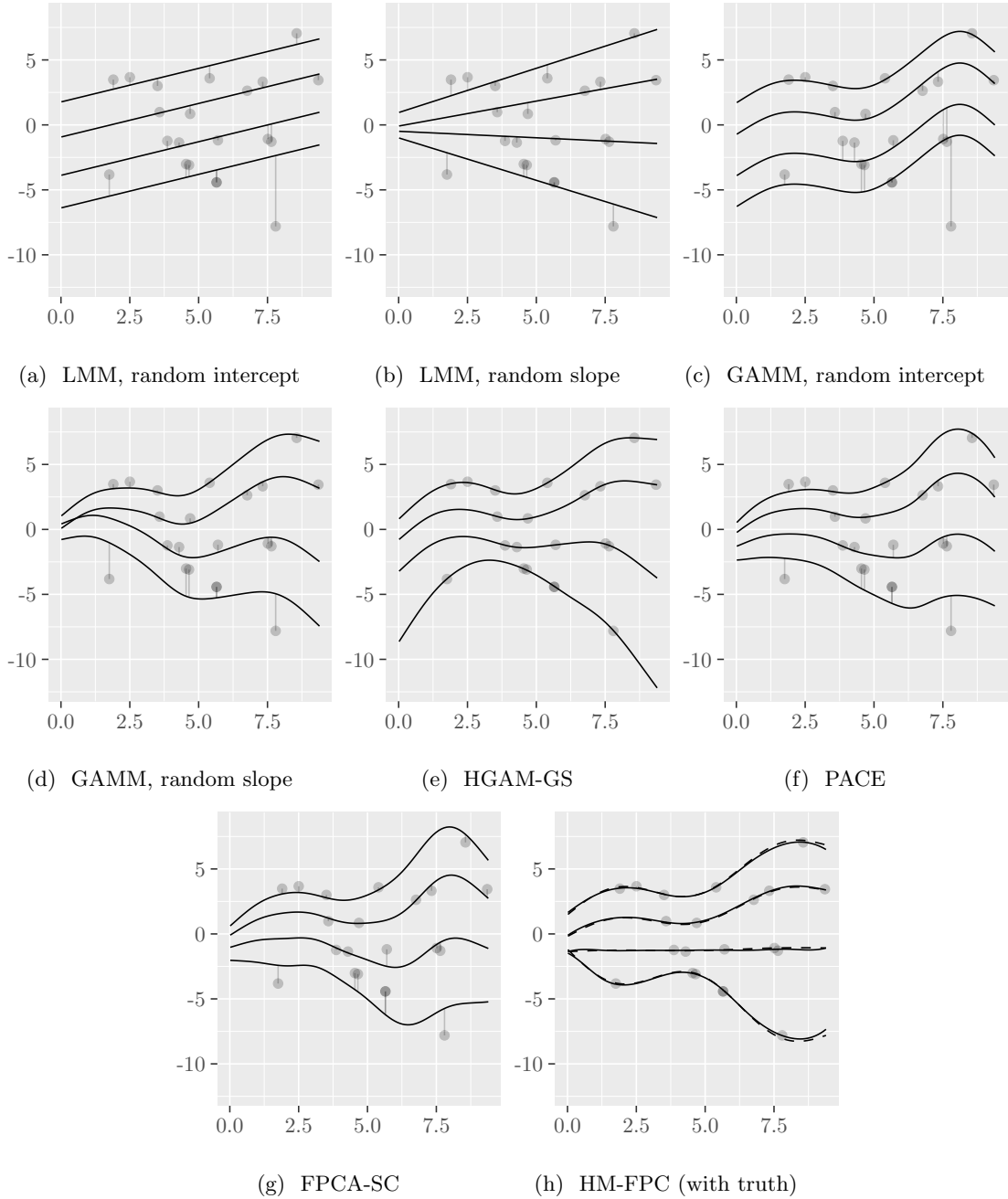


Figure 1: A subset of four fitted trajectories, found by fitting various models to a common simulated dataset (with 100 subjects and 5 observations per subject). The curved lines are the fitted trajectories, the points show data, and the vertical lines show the residual errors in the fitted trajectories. The true trajectories used to simulate the data are shown as dashed lines in h.

trajectories are close to the truth, but the estimates are less accurate for other individuals plotted. The confidence intervals cover the true trajectories for the first three individuals plotted, but not for the fourth individual. The fourth plotted individual is atypical, and the average coverage for all 100 individuals across the plotted interval $(0, 10)$ is 93% for this example, close to the nominal level.

In some cases, where there is little common structure between individuals, we cannot expect to do much better than HGAM-GS. However, there often are structural similarities in shapes of trajectories, beyond the level of smoothness. This motivates the use of functional principal components analysis, which has the potential to enable improved estimation and reduced uncertainty by exploiting these structural similarities.

2.2 Functional principal components analysis

Functional principal components analysis enables the identification and exploitation of similarities between individual trajectories, by modelling each trajectory as a population mean plus a subject-specific combination of a small number of unknown functions

The Karhunen-Loève decomposition tells us we may always write

$$\mu_i(t) = f_0(t) + \sum_{k=1}^{\infty} u_{ki} f_k(t), \quad (2)$$

where u_{ki} are uncorrelated random variables, with $E(u_{ki}) = 0$ and $\text{var}(u_{ki}) = \lambda_k$, ordered such that $\lambda_1 \geq \lambda_2 \geq \dots$. Here f_1, f_2, \dots are orthonormal functions, that is

$$\langle f_i, f_j \rangle = 0 \text{ for all } i \neq j \in \{1, 2, \dots\}$$

and

$$\langle f_k, f_k \rangle = 1 \text{ for all } k \in \{1, 2, \dots\}$$

where

$$\langle f, g \rangle = \int_{-\infty}^{\infty} f(t)g(t)dt.$$

The functions f_k , $k = 1, \dots$ are called the functional principal components, or eigenfunctions, of the process, and λ_k are called eigenvalues.

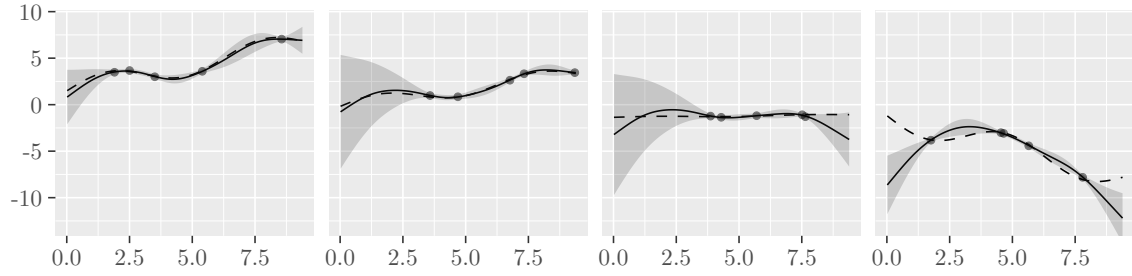
For computational simplicity and to avoid over-fitting, we might model our data by truncating the Karhunen-Loève decomposition to include only the first K functional principal components:

$$\mu_i(t) = f_0(t) + \sum_{k=1}^K u_{ki} f_k(t), \quad (3)$$

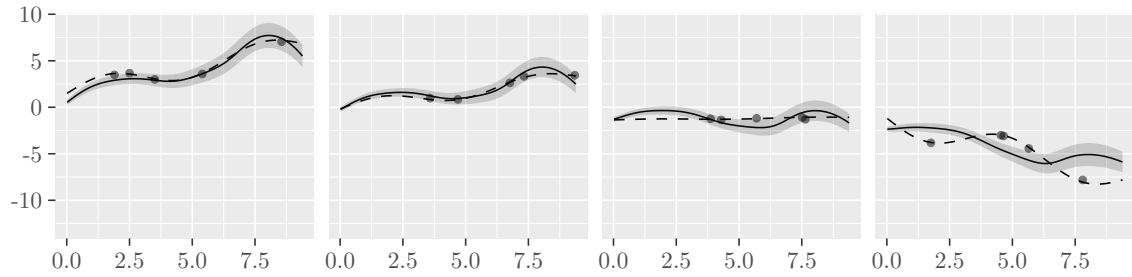
where K is the number of functional principal components included, which must be chosen based on the data. Sometimes (3) is exact: for instance, a random intercept model has $K = 1$, and a random slopes model has $K = 2$. In other cases, the model (3) will not be exact for any finite K , but a very accurate approximation to the process may be obtained with a small K , explaining the vast majority of the variation between individual trajectories. We will see an example of this in section 4.5.3, based on the SITAR model for growth curves (Cole et al., 2010).

The first methods introduced to estimate functional principal components were developed for cases with a large number of observations on each subject, made at a common dense grid of time points, as is typically the case for functional data. In longitudinal data, the observation times may be irregular and different for each subject, and the number of observations per subject is often relatively small.

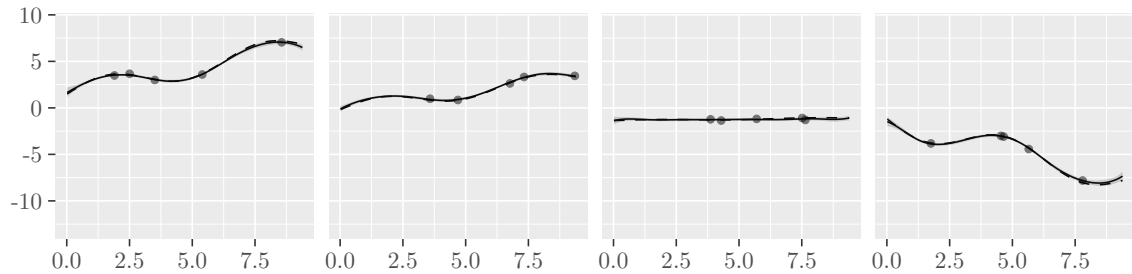
The link between functional data analysis and longitudinal data analysis was described by Yao et al. (2005), who developed the PACE (principal components analysis through conditional expectation) method for estimating the functional principal components for longitudinal data. PACE is a two-step approach: first the mean f_0 and functional principal components $f_1, f_2 \dots$ are estimated, then the rest of the model is fitted as if these estimated functions were fixed. The global mean f_0 is estimated by pooling across the subjects and fitting a smooth curve. The functional



(a) HGAM-GS (RMISE 2.36; mean CI width 1.99; coverage 93%)



(b) PACE (RMISE 2.91; mean CI width 1.68; coverage 66%)



(c) HM-FPC (RMISE 0.34; mean CI width 0.39; coverage 97%)

Figure 2: Fitted trajectories with 95% pointwise confidence intervals, for the same subset of four individuals used in Figure 1. Fitted trajectories are shown as solid lines, confidence intervals as shaded regions and data as points. The true trajectories used to generate the data are overlaid as dashed lines. The captions summarise the performance of methods averaged across all 100 individuals, in the plotted interval $(0, 10)$, in terms of root mean integrated squared error (RMISE) of fitted trajectories and average width and pointwise coverage of confidence intervals.

principal components are estimated from a smoothed version of the estimated covariance function. There are various approaches to do this smoothing: PACE uses kernel smoothing, while Di et al. (2009) and Goldsmith et al. (2013) develop functional principal components analysis by smoothed covariance (FPCA-SC), which uses penalised splines to smooth the covariance. PACE is available through the `fdapace` R package (Zhou et al., 2022), while FPCA-SC is available through the `fpca.sc` function the `refund` R package (Goldsmith et al., 2023). These methods involve two smoothing parameters: one for smoothing the mean, and another for smoothing the covariance. The number of functional principal components K must also be chosen, e.g. to explain a certain proportion of the variation, or by other criteria such as AIC or BIC.

As well as estimating the trajectories $\mu_i(\cdot)$, it is important to be able to quantify the uncertainty in these estimates. Goldsmith et al. (2013) point out that this is problematic for two-step approaches, because these methods do not take into account uncertainty in the estimated functional principal components.

Figures 1f and 1g show a subset of fitted trajectories for our motivating example data, for PACE and FPCA-SC respectively. In both cases, the fitted trajectories show considerable residual error. Should we trust these fitted models, and conclude there really is a large random error component? This seems unlikely given that HGAM-GS interpolates the data with little residual error, using very smooth curves.

The alternative is that these existing sparse FPCA methods are not able to estimate the functional principal components well in this example. This turns out to be the case: the data was generated from a model of form (3) with $K = 2$, with very small residual error $\sigma = 0.1$. Details of the data generating process are given in section 4.5.1. PACE and FPCA-SC perform poorly on this example, even though this should be an ideal situation for functional principal components analysis. Figure 2b shows the subset of PACE fitted trajectories with 95% pointwise confidence intervals and the true trajectories overlaid. PACE perform slightly worse than HGAM-GS in terms of root mean integrated squared error of the estimated trajectories, and coverage of PACE confidence intervals is 66%, well below the nominal level.

In this paper, we will develop a new modelling approach: hierarchical models with functional principal components (HM-FPC). The HM-FPC fitted trajectories are given in Figure 1h. The true trajectories used to simulate the data are overlaid as dashed curves: in this case, the estimated and true trajectories are very close, by contrast with all other methods. Figure 2c shows the subset of HM-FPC fitted trajectories with 95% pointwise confidence intervals and the true trajectories overlaid. The confidence intervals are much shorter than other methods (short enough to be only just visible at this scale), but retain high coverage (97%).

The results on one simulated dataset are included here to motivate the extent of improvement offered by HM-FPC. More detailed comparison is needed, and we will conduct a full simulation study to compare methods with this data generating process in section 4.5.1.

3 Hierarchical modelling with functional principal components

3.1 The model

For some K and functions f_0, f_1, \dots, f_K , we use model (1) with the individual trajectories assumed to be of the form

$$\mu_i(t) = f_0(t) + \sum_{k=1}^K u_{ik} f_k(t), \quad (4)$$

where u_{ik} are independent and identically distributed $N(0, 1)$ random variables. Here f_0, f_1, \dots, f_k and σ^2 are all unknown quantities which must be estimated. For now, we view K as fixed, but will describe methods to choose the value of K in section 3.7.

To make the model identifiable, we must impose some constraints on f_1, \dots, f_K . Motivated by the Karhunen-Loève decomposition (2), we enforce the constraint that f_1, \dots, f_K must be orthogonal functions, that is

$$\langle f_i, f_j \rangle = 0 \text{ for all } i \neq j \in \{1, \dots, K\}. \quad (5)$$

We enforce orthogonality rather than orthonormality because we assume that random effects u_{ik} have unit variance. This is equivalent to modelling $u_{ik} \sim N(0, \lambda_k)$, and enforcing orthonormality. The eigenvalues associated with our model can be found as $\lambda_k = \langle f_k, f_k \rangle = \|f_k\|^2$.

With the orthogonality constraint, the model is nearly identifiable, up to two simple types of transformations of the functional principal components. We can permute the order of f_1, \dots, f_K , or for any k change f_k for $-f_k$ and each u_{ik} for $-u_{ik}$, without altering the overall process. In theory, we could add extra constraints to make the model fully identifiable: ordering f_1, \dots, f_K by size, so that

$$\|f_1\| \geq \|f_2\| \geq \dots \geq \|f_K\|, \quad (6)$$

and deciding on the sign of f_k by insisting that

$$\int f_k(t) dt \geq 0. \quad (7)$$

In practice, we do not enforce these additional constraints, although our optimisation method nearly always gives estimated f_k in order of size, meeting (6). If necessary, it is straightforward to transform and solutions to meet constraints (6) and (7), by permutation and changes of sign.

For $k = 0, \dots, K$, write $f_{ki} = (f_k(t_{i1}), \dots, f_k(t_{in_i}))^T$ for the vector which evaluates the function f_k at each time point for subject i . The joint distribution of $Y_i = (Y_{i1}, \dots, Y_{in_i})$ in model (4) is

$$Y_i \sim N_{n_i}(f_{0i}, \Sigma(\sigma^2, f_{1i}, \dots, f_{Ki})),$$

where

$$\Sigma(\sigma^2, f_{1i}, \dots, f_{Ki}) = \sigma^2 I + \sum_{k=1}^K f_{ki} f_{ki}^T. \quad (8)$$

The likelihood of the model (4) is therefore

$$L(f_0, f_1, \dots, f_K, \sigma^2) = \prod_{i=1}^d \phi_{n_i}(y_i; f_{0i}, \Sigma(\sigma^2, f_{1i}, \dots, f_{Ki})),$$

where $\phi_n(\cdot; \mu, \Sigma)$ is the probability density function of the $N_n(\mu, \Sigma)$ distribution, and the log-likelihood is

$$\ell^f(f_0, f_1, \dots, f_K, \sigma^2) = \sum_{i=1}^d \log \phi_{n_i}(y_i; f_{0i}, \Sigma(\sigma^2, f_{1i}, \dots, f_{Ki})). \quad (9)$$

We include the superscript f to clarify that here we parameterise the process by the functions f_0, f_1, \dots, f_K , as we later consider log-likelihoods under alternative parameterisations.

To avoid over-fitting, we penalise the expected wiggleness of each individual trajectory $\mu_i(\cdot)$. We write

$$w(f) = \int_{-\infty}^{\infty} f''(t)^2 dt$$

for the wiggleness of a function $f(\cdot)$, and let $w_E = E[w(\mu_i)]$ be the expected wiggleness of μ_i , where μ_i are random variables as described by (4). There is a simple formula for the expected wiggleness:

Claim 1. *We have*

$$w_E = w(f_0) + \sum_{j=1}^K w(f_j).$$

All proofs are given in Appendix A. We write $w_E = w_E(f_0, f_1, \dots, f_K)$, to make the dependence on the functions f_0, f_1, \dots, f_K explicit.

We maximise the penalised log-likelihood

$$\ell_p^f(f_0, f_1, \dots, f_K, \sigma^2) = \ell^f(f_0, f_1, \dots, f_K, \sigma^2) - \frac{\gamma}{2\sigma^2} w_E(f_0, f_1, \dots, f_K), \quad (10)$$

where γ is a smoothing parameter. For now, we will focus on estimating the model parameters for fixed γ , and return to the problem of choosing γ in section 3.7, where we also justify dividing the smoothing parameter by $2\sigma^2$.

To estimate the unknown quantities, we could choose f_0, f_1, \dots, f_K and σ^2 to maximise $\ell_p^f(f_0, f_1, \dots, f_K)$, subject to the constraint (5), that f_1, \dots, f_K are orthogonal functions.

This very general form of the optimisation problem is not yet feasible to use in practice. It involves infinite-dimensional optimisation over all possible functions f_0, f_1, \dots, f_K : in section 3.2 we will reduce this to a finite-dimensional problem by writing the f_j in terms of basis functions. A challenging constrained optimisation problem still remains, due to the orthogonality constraint on f_1, \dots, f_K . In section 3.3 we will address this by creating a new parameterisation for the problem which ensures orthogonality between f_1, \dots, f_K .

3.2 Spline basis

We write

$$f_j(t) = \sum_{l=1}^{n_B} \beta_{jl} b_l(t) = \beta_j^T b(t),$$

for $j = 0, 1, \dots, K$, where $b_l(\cdot)$ are cubic spline basis functions, $b(t) = (b_1(t), \dots, b_{n_B}(t))^T$ is a vector of basis functions evaluated at t , and $\beta_j = (\beta_{j1}, \dots, \beta_{jn_B})^T$ is the vector of coefficients for f_j . In this form, the unknown quantities to estimate are $\beta_0, \beta_1, \dots, \beta_K$ and σ^2 .

The log-likelihood has the same form as (9), where the values of $f_{ki} = (f_k(t_{i1}), \dots, f_k(t_{in_i}))^T$ depend on β_k through

$$f_k(t_{ij}) = \beta_k^T b(t_{ij}).$$

Write $X^{(i)}$ as a $n_i \times n_B$ design matrix for the basis for the i th subject, with j th row $b(t_{ij})$. Then we may write $f_{ki}(\beta_k) = X^{(i)}\beta_k$, and the log-likelihood is

$$\ell^\beta(\beta_0, \beta_1, \dots, \beta_K, \sigma^2) = \sum_{i=1}^d \log \phi_{n_i}(y_i; f_{0i}(\beta_0), \Sigma(\sigma^2, f_{1i}(\beta_1), \dots, f_{Ki}(\beta_K))).$$

We will choose our basis functions to be orthonormal, such that

$$\langle b_i, b_i \rangle = 1 \text{ and } \langle b_i, b_j \rangle = 0 \text{ for all } i \neq j.$$

We use the `orthogonalsplinebasis` R package (Redd, 2022) to do this. Claim 2 says that we can obtain a set of orthogonal functions from an orthonormal basis by choosing a set of orthogonal coefficient vectors.

Claim 2. *Suppose that b_1, \dots, b_{n_B} are an orthonormal basis, and $f_j(t) = \sum_{l=1}^{n_B} \beta_{jl} b_l(t)$. Then the functions f_1, \dots, f_K are orthogonal if and only if the coefficient vectors β_1, \dots, β_K are orthogonal, that is, if*

$$\langle \beta_i, \beta_j \rangle = 0, \text{ for all } i \neq j \in \{1, \dots, K\} \quad (11)$$

where $\langle \beta_i, \beta_j \rangle = \beta_i^T \beta_j$ is the usual inner product for vectors.

Finding the wiggleness of each f_j from the spline basis is straightforward: there is a matrix S such that $w(f_j) = \beta_j^T S \beta_j$. Given the coefficient vectors $\beta_0, \beta_1, \dots, \beta_K$, the expected wiggleness may be written

$$w_E = \sum_{j=0}^K \beta_j^T S \beta_j.$$

We will write $w_E = w_E(\beta_0, \beta_1, \dots, \beta_K)$ to make the dependence on the coefficient vectors explicit.

We could therefore estimate the unknown parameters $\beta_0, \beta_1, \dots, \beta_K$ and σ^2 by maximising the penalised log-likelihood

$$\ell_p^\beta(\beta_0, \beta_1, \dots, \beta_K, \sigma^2) = \ell^\beta(\beta_0, \beta_1, \dots, \beta_K, \sigma^2) - \frac{\gamma}{2\sigma^2} w_E(\beta_0, \beta_1, \dots, \beta_K) \quad (12)$$

subject to the constraint that β_1, \dots, β_K are orthogonal vectors. The constraint makes this a challenging optimisation problem, and in section 3.3 we will develop a new parameterisation which ensures the component vectors β_1, \dots, β_K are orthogonal, to remove the constraint at the optimisation stage.

3.3 Orthogonality transform

In this section we describe a reparameterisation $\alpha_1, \dots, \alpha_K$ such that any orthogonal set of vectors β_1, \dots, β_K may be obtained for some choice of the α_k s. In combination with the orthonormal spline basis from section 3.2, this will enable us to parameterise the set of orthogonal functions f_1, \dots, f_k , without the need to place any constraints on the values of the new parameters $\alpha_1, \dots, \alpha_K$.

We do not place any constraints on β_1 , and let $\beta_1 = \alpha_1$, for any $\alpha_1 \in \mathbb{R}^{n_B}$. For each $k > 1$, we need to ensure that β_k is orthogonal to each of $\beta_1, \dots, \beta_{k-1}$, leading to $k - 1$ constraints, so we take $\alpha_k \in \mathbb{R}^{n_B - k + 1}$. We may rewrite the constraint that β_k is orthogonal to each of $\beta_1, \dots, \beta_{k-1}$ in matrix-vector form, as

$$B_{k-1}^T \beta_k = 0, \quad (13)$$

where B_{k-1} is the $n_B \times (k - 1)$ matrix with columns $\beta_1, \dots, \beta_{k-1}$. To find β_k from α_K and $\beta_1, \dots, \beta_{k-1}$, we follow a general recipe described in section 1.8.1 of Wood (2017):

1. Find a QR decomposition of B_{k-1} , as $B_{k-1} = Q_{k-1}R_{k-1}$, where Q_{k-1} is an orthogonal matrix and R_{k-1} is upper triangular.
2. Partition $Q_{k-1} = (S_{k-1} : T_{k-1})$ so that T_{k-1} contains the final $n_B - k + 1$ columns of Q_{k-1} .
3. Let

$$\beta_k = T_{k-1} \alpha_k.$$

For any $\alpha_k \in \mathbb{R}^{n_B - k + 1}$, this give a β_k meeting the orthogonality constraint (13).

We may find the penalised likelihood under our new parameterisation by first finding $\beta = (\beta_1, \dots, \beta_K)$ from $\alpha = (\alpha_1, \dots, \alpha_K)$ then substituting into the penalised log-likelihood (12) for $(\beta_0, \beta, \sigma^2)$, to give

$$\ell_p^\alpha(\beta_0, \alpha, \sigma^2) = \ell_p^\beta(\beta_0, \beta(\alpha), \sigma^2).$$

3.4 Maximising the penalised log-likelihood

For numerical stability, we maximise the penalised log-likelihood over $\log \sigma$ rather than σ^2 . The full set of parameters is $\theta = (\beta_0, \alpha, \log \sigma)$, with penalised log-likelihood

$$\ell_p(\theta) = \ell_p(\beta_0, \alpha, \log \sigma) = \ell_p^\beta(\beta_0, \alpha, \exp(2 \log \sigma)). \quad (14)$$

We find the maximum penalised likelihood estimate $\hat{\theta}$ by maximising $\ell_p(\theta)$ from (14) over θ . In practice, we do this by first fitting the model with $K = 0$, then increasing K one at a time, using the parameter values from the previous fit to give starting values for the optimisation.

We use the BFGS method to maximise the penalised log-likelihood. For speed, it is important to have access to the gradient of the penalised log-likelihood, which would be difficult to find by hand because of the complexity of the transformation in 3.3. We used automatic differentiation to obtain the gradient, by using the Stan Math C++ library in R (Stan Development Team, 2020).

3.5 Estimating the individual trajectories

Given the maximum penalised likelihood estimate $\hat{\theta}$, we can estimate the individual trajectories as

$$\hat{\mu}_i(t) = \hat{f}_0(t) + \sum_{k=1}^K \hat{u}_{ki} \hat{f}_k(t),$$

where $\hat{f}_k(t) = \hat{\beta}_k^T b(t)$, where $\hat{\beta}_k = \beta_k(\hat{\theta})$, and we estimate $u_i = (u_{i1}, \dots, u_{iK})^T$ by

$$\hat{u}_i = \hat{\Sigma}_i^{-1}(y_i - \hat{f}_0i),$$

where $\hat{\Sigma}_i = \Sigma(\hat{\sigma}^2, \hat{f}_{1i}, \dots, \hat{f}_{Ki})$ from (8).

3.6 Confidence intervals

We express the uncertainty in our estimated mean curves $\hat{\mu}_i(t)$ through pointwise confidence intervals.

We may always express each individual trajectory in terms of the fixed set of basis functions $b(\cdot)$. For fixed β and u , we may write

$$\mu_i(t) = \beta_0^T b(t) + \sum_{k=1}^K u_{ik} \beta_k^T b(t) = (\beta_0 + \sum_{k=1}^K u_{ik} \beta_k)^T b(t) = \delta_i^T b(t)$$

where

$$\delta_i = \beta_0 + \sum_{k=1}^K u_{ik} \beta_k$$

are the basis coefficients for μ_i , which depend on β and u_i .

To find a pointwise confidence interval for $\mu_i(t)$, we use a parametric bootstrap approach. We will first find a parametric bootstrap sample $\{\delta_i^{(1)}, \dots, \delta_i^{(n_S)}\}$ for the basis coefficients δ_i of the individual trajectories.

For the fitted model (with K and γ treated as fixed at their chosen values), we first find the Hessian matrix H of the penalised log-likelihood at the maximum penalised likelihood estimate $\hat{\theta}$, and find $V = -H^{-1}$. For each $j = 1, \dots, n_S$, to find the sample $\delta^{(j)}$, we:

1. Generate $\theta^{(j)} \sim N_p(\hat{\theta}, V)$.
2. Reparameterise out of the orthogonal parameterisation, to find $\beta_k^{(j)} = \beta_k(\theta^{(j)})$. Write $f_k^{(j)}(t) = [\beta_k^{(j)}]^T b(t)$.
3. For each subject $i = 1, \dots, d$:
 - (a) Find $f_{0i}^{(j)}, f_{1i}^{(j)}, \dots, f_{Ki}^{(j)}$, where $f_{ki} = (f_k^{(j)}(t_{i1}), \dots, f_k^{(j)}(t_{in_i}))^T$, is the vector which evaluates the function $f_k^{(j)}$ at each time point for subject i .
 - (b) Find $\Sigma_i^{(j)} = \Sigma([\sigma^2]^{(j)}, f_{1i}^{(j)}, \dots, f_{Ki}^{(j)})$ using (8), and $\hat{u}_i^{(j)} = (\Sigma_i^{(j)})^{-1} (y_i - f_{0i}^{(j)})$.
 - (c) Sample $u_i^{(j)} | \theta^{(j)}, y, \sim N(\hat{u}_i^{(j)}, \Sigma_i^{(j)})$.
 - (d) Find

$$\delta_i^{(j)} = \beta_0^{(j)} + \sum_{k=1}^K u_{ik}^{(j)} \beta_k^{(j)}$$

4. Return $\delta^{(j)} = (\delta_1^{(j)}, \dots, \delta_d^{(j)})$.

Given $\{\delta_i^{(1)}, \dots, \delta_i^{(n_S)}\}$, we may then find a confidence interval for $\mu_i(t)$ (at any time point t) by finding

$$[\mu_i(t)]^{(j)} = \delta_i^{(j)} b(t)$$

for each sample $j = 1, \dots, n_S$, then using appropriate quantiles of $\{[\mu_i(t)]^{(1)}, \dots, [\mu_i(t)]^{(n_S)}\}$ (e.g. the 2.5% and 97.5% quantiles for a 95% interval).

In addition to confidence intervals about μ_i , we could also use the sample $\delta^{(j)}$ to find confidence intervals for other quantities of interest. For instance, we can find confidence intervals for the derivative of the individual trajectory by finding

$$[\mu_i'(t)]^{(j)} = \delta_i^{(j)} b'(t).$$

This process does not allow for uncertainty in the tuning parameters K and γ , so there may be some potential for under-coverage. However, we will see that the confidence intervals have close to nominal coverage in simulation studies.

3.7 Choosing the tuning parameters

3.7.1 Choosing the number of functional principal components K

For a fixed smoothing parameter γ , we find that the fit eventually stabilises as we increase the number of functional principal components K , with $\hat{\lambda}_K = \|\hat{f}_K\|^2$ approaching zero. We could take K very large, and still get a good fit, but with lots of unimportant functional principal components, with $\hat{\lambda}_k \approx 0$. For computational reasons, we prefer K to choose as small as possible while including all of the important functional principal components.

To do this, we use the fraction of variance explained. For each candidate K , we estimate the error variance $\hat{\sigma}_K^2$. There is a residual variance which cannot be explained by variation in the individual trajectories, which we write as $\hat{\sigma}_\infty^2 = \lim_{K \rightarrow \infty} \hat{\sigma}_K^2$. The non-residual variance for each K is $\hat{\sigma}_K^2 - \hat{\sigma}_\infty^2$. The fraction of variance explained is

$$\text{FVE}(K) = \frac{\hat{\sigma}_0^2 - \hat{\sigma}_K^2}{\hat{\sigma}_0^2 - \hat{\sigma}_\infty^2}$$

We aim to choose the smallest K so that $\text{FVE}(K) > t_{\text{FVE}}$, for some threshold t_{FVE} , close to 1. In all the later examples we use $t_{\text{FVE}} = 0.999$.

We cannot calculate $\hat{\sigma}_\infty^2$, since we do not fit the model with infinitely large K . For sufficiently large K , we will have $\hat{\sigma}_K^2 \approx \hat{\sigma}_\infty^2$. Starting with $K_{\max} = 2$, fit the model for all $K \leq K_{\max}$, and use $\hat{\sigma}_{K_{\max}}^2$ in place of $\hat{\sigma}_\infty^2$, to give

$$\text{FVE}(K; K_{\max}) = \frac{\hat{\sigma}_0^2 - \hat{\sigma}_K^2}{\hat{\sigma}_0^2 - \hat{\sigma}_{K_{\max}}^2}.$$

We check whether $\text{FVE}(K_{\max} - 1; K_{\max}) > t_{\text{FVE}}$, and choose $K = K_{\max} - 1$ if so. If not, we increase K_{\max} by one, refit the model with $K = K_{\max}$, and repeat the process until we have a sufficiently large fraction of variance explained.

3.7.2 Choosing the smoothing parameter γ

We choose the smoothing parameter γ to maximise an approximate marginal likelihood. To do this, we must first consider a Bayesian interpretation of the penalty term.

We may rewrite the penalty term in (12) as

$$-\frac{\gamma}{2\sigma^2} w_E = \sum_{j=0}^K -\frac{\gamma}{2\sigma^2} \beta_j^T S \beta_j.$$

We use the equivalence between penalised likelihood estimation with penalty

$$-\frac{\gamma}{2\sigma^2} \beta_k^T S \beta_k$$

and maximum a posteriori estimation with improper Bayesian prior

$$\beta_k \sim N\left(0, \frac{\sigma^2}{\gamma} S^-\right), \quad (15)$$

an improper normal prior where S^- is the pseudo-inverse of the matrix S , since S is not of full rank (Wood, 2017, section 4.2.4).

The prior for β_0 is given by (15). Since we reparameterise $\beta = (\beta_1, \dots, \beta_K)$ in terms of $\alpha = (\alpha_1, \dots, \alpha_K)$, we seek a prior for α such that if α has this distribution then $\beta_k = \beta_k(\alpha)$ has distribution (15) for $k = 1, \dots, K$.

We may achieve this by letting

$$\alpha_1 \sim N\left(0, \frac{\sigma^2}{\gamma} S^-\right)$$

and

$$\alpha_k | \alpha_1, \dots, \alpha_{k-1} \sim N \left(0, \frac{\sigma^2}{\gamma} S_k^- \right), \quad \text{for } k = 2, \dots, K,$$

where

$$S_k = T_{k-1}^T S T_{k-1}.$$

The matrices T_{k-1} are defined in step (2) of the transformation in section 3.3, and depend on $\alpha_1, \dots, \alpha_{k-1}$.

Since we optimise our penalised log-likelihood over $\theta = (\beta_0, \alpha_1, \dots, \alpha_K, \log \sigma)^T$, we will also include a prior on $\log \sigma$, which we describe shortly. Our penalty over θ is

$$\text{pen}(\theta | \gamma) = -\frac{\gamma}{2\sigma^2} \beta_0^T S \beta_0 - \sum_{k=1}^K \alpha_k S_k^T \alpha_k$$

We then rewrite the log prior as the penalty plus a remainder term, as

$$\log \pi(\theta | \gamma) = \text{pen}(\theta | \gamma) + r(\theta, \gamma).$$

If we choose the improper prior $\pi(\log \sigma) \propto \sigma^{-2R}$ for $\log \sigma$, where $R = \sum_{k=0}^K r_k$ and $r_k = \text{rank}(S_k) = \min\{n_B - 2, n_B - k + 1\}$, then the remainder term is

$$r(\theta, \gamma) = \frac{1}{2} \sum_{k=0}^K \log |S_k|_+ + R(\log \gamma - 1).$$

At first sight, it appears that there is no dependence on θ in the remainder $r(\theta, \gamma)$, which would lead to an exact match between the maximum a-posteriori estimate and the penalised likelihood estimate. However, there is a small dependence on α , since S_K depends on $\alpha_1, \dots, \alpha_{K-1}$, so the maximum a-posteriori estimate will differ slightly from the penalised likelihood estimate.

We choose γ to maximise a quantity based on the marginal likelihood for γ ,

$$c_\gamma = \int \pi_{\text{unnorm}}(\theta, \gamma | y) d\theta \quad (16)$$

where

$$\pi_{\text{unnorm}}(\theta, \gamma | y) = f(y | \theta) \pi(\theta | \gamma).$$

Making a Laplace approximation to (16) gives an approximate log-marginal likelihood

$$\log \hat{c}_\gamma = \log \pi_{\text{unnorm}}(\theta_{\text{MAP}}(\gamma), \gamma) + \frac{p}{2} \log(2\pi) - \frac{1}{2} |\log H_{\text{MAP}}(\gamma)|, \quad (17)$$

where $\theta_{\text{MAP}}(\gamma)$ is the maximum a-posteriori estimate for θ given γ , $H_{\text{MAP}}(\gamma)$ is the Hessian of $\log \pi_{\text{unnorm}}(\theta | y)$ at $\theta_{\text{MAP}}(\gamma)$ and $p = \dim(\theta)$.

We find a further approximation to the marginal likelihood by replacing $\theta_{\text{MAP}}(\gamma)$ by the penalised likelihood estimate $\hat{\theta}(\gamma)$ in (17), also replacing $H_{\text{MAP}}(\gamma)$ by $\hat{H}(\gamma)$, the Hessian of the penalised log-likelihood at its maximum, which gives our approximate log marginal likelihood criterion

$$\begin{aligned} \log \tilde{c}_\gamma &= \log \pi_{\text{unnorm}}(\hat{\theta}(\gamma), \gamma) + \frac{p}{2} \log(2\pi) - \frac{1}{2} |\log \hat{H}(\gamma)|, \\ &= \ell_p(\hat{\theta}(\gamma), \gamma) + r(\hat{\theta}(\gamma), \gamma) + \frac{p}{2} \log(2\pi) - \frac{1}{2} |\log \hat{H}(\gamma)|. \end{aligned} \quad (18)$$

In examples, we find that maximising this criterion tends to give an appropriate value of γ . The inference is typically not sensitive to the precise value of γ . Further study of the properties of the criterion would be useful, and is left for future work.

In theory, the same marginal likelihood criterion (18) could be optimised over K as well as γ . However, computing the marginal likelihood criterion requires us to first find the Hessian matrix at the maximum of the penalised log-likelihood, which is relatively computationally expensive. We reduce the computational burden by finding a marginal likelihood just once for each γ , choosing K given γ as described in section 3.7.1.

3.8 Population-level inference

The model (4) for the trajectories is a Gaussian process. At population-level, averaging over u_i , we write $\mu_i(\cdot) \sim \mathcal{GP}(m(\cdot), C(\cdot, \cdot))$ with mean function $m(t) = E(\mu_i(t)) = f_0(t)$ and covariance function

$$C(s, t) = \text{Cov}(\mu_i(s), \mu_i(t)) = \sum_{k=1}^K f_k(s)f_k(t). \quad (19)$$

Substituting the estimated mean and function principal components, we can estimate the population-level process as $\mathcal{GP}(\hat{m}(\cdot), \hat{C}(\cdot, \cdot))$, where

$$\hat{m}(t) = \hat{f}_0(t); \quad \hat{C}(s, t) = \sum_{k=1}^K \hat{f}_k(s)\hat{f}_k(t).$$

We call this the FPC method for population-level inference.

Alternatively, we can average the sample mean and covariance of the individual trajectories,

$$\tilde{m}(t) = \frac{1}{d} \sum_{i=1}^d \hat{\mu}_i(t); \quad \tilde{C}(s, t) = \frac{1}{d} \sum_{i=1}^d (\hat{\mu}_i(s) - \tilde{m}(s)) (\hat{\mu}_i(t) - \tilde{m}(t)), \quad (20)$$

and estimate the population-level process as $\mathcal{GP}(\tilde{m}(\cdot), \tilde{C}(\cdot, \cdot))$. We call this the empirical method for population-level inference.

4 Comparison of methods

4.1 Introduction

Next we compare the hierarchical modelling with functional principal components approach against existing methods.

From a theoretical perspective, we briefly consider asymptotics as the number of individuals $d \rightarrow \infty$. If the model (4) is correct for some $K = K_0$, and we choose $K \geq K_0$ and any fixed γ , the estimated model parameters will be asymptotically consistent and fully efficient, as inference is based on the (correctly-specified) likelihood, and the log-likelihood dominates the penalty term asymptotically. Assuming that the mean and functional principal components may be written in terms of the chosen spline basis, this means that HM-FPC provides consistent and fully efficient inference for the mean f_0 , functional principal components f_1, \dots, f_K and covariance function C (which may be expressed in terms of the functional principal components, by (19)). PACE has also been shown to consistently estimate these quantities (Yao et al., 2005), but is not fully efficient.

To compare methods empirically, we simulate from model (1), with a wide range of different choices for the true trajectories μ_i . The various processes used to generate the data are described in section 4.2. For each choice, we generate 100 datasets, then use a range of methods to estimate the trajectories μ_i . A common set of methods are used for estimation in each case, as described in section 4.3. The metrics we use to compare the quality of inference from each method are described in section 4.4.

4.2 Data generating processes

For ease of reference later on, we give short names to our chosen data generating processes (highlighted below in bold type). The models used to simulate trajectories are:

1. **2FPC**: a model with $K = 2$ functional principal components. We have already studied one simulated dataset from this process as a motivating example in section 2.1. Details and results are given in section 4.5.1.
2. **LMM-RI**: a simple linear mixed model with random intercepts. Details and results are given in section 4.5.2.

3. **SITAR**: Cole et al. (2010) describe a model for growth curves called SuperImposition by Translation And Rotation (SITAR). We generate data from SITAR as an example of a realistic process which is not expressible in terms of a finite number of functional principal components, but for which there are nonetheless strong structural similarities between trajectories. In the example we consider, 99.7% of the variability is explained by $K = 3$ functional principal components. Details and results are given in section 4.5.3.

We study the impact of varying the number of individuals, d , and the number of observations on each individual, n_i . For each case, we generate 100 datasets from each of 18 processes, given by all possible combinations of $d \in \{50, 100, 200, 300, 400, 500\}$ and $n_i \in \{3, 5, 10\}$ (with an equal number of observations on each subject).

4.3 Estimation methods

For ease of reference later on, we give short names to our chosen estimation methods (highlighted below in bold type). The methods used are:

1. **HGAM-GS**: A hierarchical generalised additive model with a common population mean and shared smoothing parameters, as described in Pedersen et al. (2019). We used the `bam` function in `mgcv` to fit the model. This method is computationally expensive for large number of individuals (d), so we only used it in cases with $d \leq 300$.
2. **PACE** (Yao et al., 2005), through the `FPCA` function in the `fdapace` R package, selecting K by using BIC. In preliminary simulation runs, we tried other methods to select K (by AIC, or to explain some fraction of the variance) and found BIC typically gave the best results of the available methods. We use generalised cross validation to select bandwidths for smoothing the mean and covariance functions (as this gave better results than the default choice), and default values for other parameters.
3. **HM-FPC**: the proposed hierarchical model with functional principal components. We use the methods for choosing K and γ described in section 3.7, with $t_{\text{FVE}} = 0.999$ for the FVE threshold.

In preliminary simulation runs, we also included the FPCA-SC method, through the `fpca.sc` function in the `refund` R package. The performance with fixed K was typically similar to PACE, but the methods available to select K (to explain some fraction of the variance) did not work as well as BIC in PACE. Since R occasionally crashed when fitting a model with `fpca.sc` for large d , we decided not to include this method in the full simulation studies. We also used the method of Goldsmith et al. (2013), through the `ccb.fpc` function in `refund`, in preliminary runs, but it appeared to give worse estimates than the FPCA-SC method in the cases we considered, with extremely large confidence intervals. Since this method was also more computationally expensive than the others, we decided not to include it in the full simulation studies.

4.4 Measures used for comparisons

4.4.1 Individual-level inference

We compare the quality of inference about the individual trajectories by using the mean integrated squared error for each estimate of the trajectories $\hat{\mu} = (\hat{\mu}_1, \dots, \hat{\mu}_d)$, across the range of times observed in the data. We define the integrated squared error for subject i as

$$\text{ISE}(\hat{\mu}_i) = \int_{t_{\min}}^{t_{\max}} [\hat{\mu}_i(t) - \mu_i(t)]^2 dt,$$

where $t_{\min} = \min_{i,j} \{t_{ij}\}$ and $t_{\max} = \max_{i,j} \{t_{ij}\}$. The mean integrated squared error is

$$\text{MISE}(\hat{\mu}) = \frac{1}{d} \sum_{i=1}^d \text{ISE}(\hat{\mu}_i).$$

We then find the MISE for each of the 100 datasets generated from each process, and report the RMISE – the square root of the mean MISE across datasets – for each method.

We compute pointwise 95% confidence intervals associated with each estimated trajectory $\hat{\mu}_i$. For each dataset, we compute the average pointwise coverage and average width of these intervals, across the range of times observed in the data $[t_{\min}, t_{\max}]$. For each case, we report the average coverage and width across all 100 simulated datasets. For PACE, computing a confidence interval sometimes failed, so coverage and average width for PACE intervals are found by averaging over the subset of simulated datasets for which a PACE interval could be computed. This may lead to some bias in the reported properties of PACE confidence intervals. If the problems in producing PACE confidence intervals in `fdapace` were fixed, it would be straightforward to re-run the simulations and remove this potential bias.

For each case, it is useful to be able to examine some estimated trajectories for a typical simulation run. To do this, we first find a combined error for each run by adding up the mean integrated squared errors from all estimation methods considered. We then find the mean combined error across all runs, and define the typical simulation run as the run with combined error closest to the mean. Within this typical simulation run, we plot trajectories for a subset of five individuals, selected to show a range of combined errors. To do this, we select individuals with $(0, 0.25, 0.5, 0.75, 1)$ -quantiles of combined error (minimum, first-quartile, median, third-quartile and maximum combined error).

4.4.2 Population-level inference

In the 2FPC and LMM-RI cases, model (4) is correct for some $K = K_0$, so we use (19) to find the covariance function. In the SITAR case, model (4) is not correct for any finite K , and the population-level process is not a Gaussian process. Nonetheless, we can still compute the true mean and covariance functions, and we study the error in the estimated Gaussian process relative to a Gaussian process with these true mean and covariance functions.

For HM-FPC, two methods for population-level inference are described in Section 3.8: the FPC method and the empirical method. The FPC method may also be used with PACE, and the empirical may be used with all estimation methods.

We use the empirical method for HGAM-GS (since the FPC method is not available). For PACE and HM-FPC, we tried both the FPC and empirical methods. For HM-FPC, the results of the two methods were very similar, with the empirical method slightly outperforming the FPC method in cases with small d . For PACE, the FPC method substantially outperformed the empirical method. In simulations, we therefore report on population-level inference using the empirical method for HM-FPC and the FPC method for PACE.

To compare the true and estimated Gaussian processes, we use a Wasserstein distance. We first discretise the true and estimated Gaussian processes by considering all functions evaluated on a fine grid of time points $(t_1, \dots, t_N)^T$. Write $\mu_i = (\mu_i(t_1), \dots, \mu_i(t_N))^T$, m for the N -vector with entries $m_j = m(t_j)$ and C for the $N \times N$ matrix with entries $C_{j_1, j_2} = C(t_{j_1}, t_{j_2})$, and similarly \hat{m} and \hat{C} are the discretised versions of $\hat{m}(\cdot)$ and $\hat{C}(\cdot)$. So, in truth we have $\mu_i \sim N_N(m, C)$, and we estimate $\mu_i \sim N_N(\hat{m}, \hat{C})$. Olkin and Pukelsheim (1982) showed that the 2-Wasserstein distance between $N_N(m, C)$ and $N_N(\hat{m}, \hat{C})$ is

$$W_2(N) = \|\hat{m} - m\|_2^2 + \text{trace} \left(\hat{C} + C - 2(C^{1/2}\hat{C}C^{1/2})^{1/2} \right). \quad (21)$$

We average this, to give $\bar{W}_2 = N^{-1}W_2(N)$, which stabilises in the large- N limit. In simulation studies, we use a regular grid of $N = 100$ time points between t_{\min} and t_{\max} to calculate a 2-Wasserstein error $\bar{W}_2^{(i)}$ for each simulation run ($i = 1, \dots, n_{\text{sim}}$). We aggregate this to give the mean 2-Wasserstein error (MWE) across simulation runs,

$$\text{MWE} = \frac{1}{n_{\text{sim}}} \sum_{i=1}^{n_{\text{sim}}} \bar{W}_2^{(i)},$$

where $n_{\text{sim}} = 100$, and report the root mean 2-Wasserstein error, $\text{RMWE} = \sqrt{\text{MWE}}$.

We can write (21) as $W_2(N) = d_m^2(N) + d_C^2(N)$, where $d_m^2(N) = \|\hat{m} - m\|_2^2$ is the squared Euclidean distance between means \hat{m} and m and $d_C^2(N) = \text{trace}(\hat{C} + C - 2(C^{1/2}\hat{C}C^{1/2})^{1/2})$ is a squared distance between \hat{C} and C . Dividing by N , we have

$$\bar{W}_2 = \bar{d}_m^2 + \bar{d}_C^2,$$

where $\bar{d}_m^2 = N^{-1}d_m^2(N)$ and $\bar{d}_C^2 = N^{-1}d_C^2(N)$. Aggregating over simulation runs, the mean 2-Wasserstein error may be written $\text{MWE} = \text{MSE}_m + \text{MSE}_C$, where

$$\text{MSE}_m = \frac{1}{n_{\text{sim}}} \sum_{i=1}^{n_{\text{sim}}} \bar{d}_m^2 \quad \text{and} \quad \text{MSE}_C = \frac{1}{n_{\text{sim}}} \sum_{i=1}^{n_{\text{sim}}} \bar{d}_C^2$$

are mean squared errors in the estimated mean and covariance. We report the root mean squared errors $\text{RMSE}_m = \sqrt{\text{MSE}_m}$ and $\text{RMSE}_C = \sqrt{\text{MSE}_C}$, to understand whether the overall error in the population process is dominated by error in the mean or covariance functions.

4.5 Results

4.5.1 2FPC

We simulate from a model which may be written in form (4) with $K = 2$, but for which the variation between individual trajectories is not fully explained by changing the intercept and slope. We let

$$\mu_i(t) = (1 + u_{i1})h(t) + u_{i2},$$

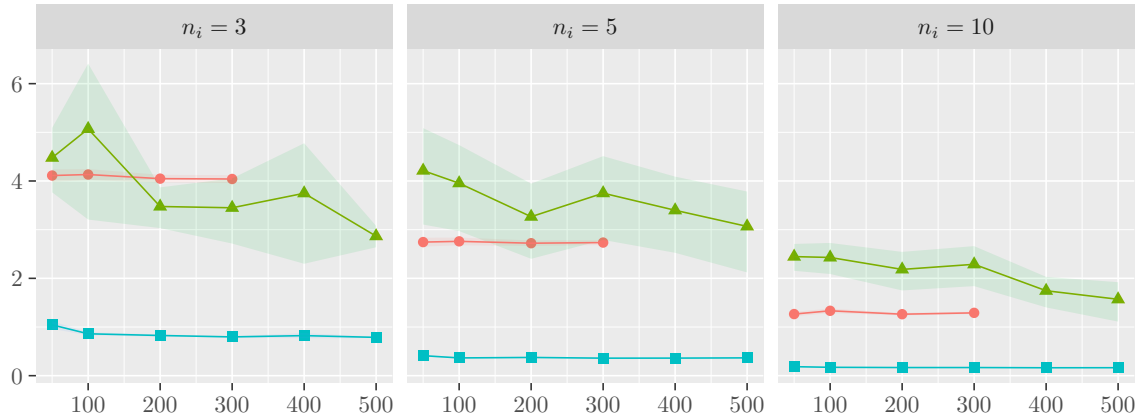
where $h(t) = x/2 + \sin(x)$ and u_{i1} and u_{i2} are independent $N(0, 1)$ random variables. We generate t_{ij} uniformly on the interval $[0, 3\pi]$. The observation error has standard deviation $\sigma = 0.1$. We have already studied one simulated dataset from this process as a motivating example in section 2.1, with $d = 100$ and $n_i = 5$. We now extend this to a full simulation study, for 18 processes of this form, given by all possible combinations of $d \in \{50, 100, 200, 300, 400, 500\}$ and $n_i \in \{3, 5, 10\}$.

Figure 3a shows the root mean integrated squared error for each choice of number of individuals d and number of observations on each individual n_i . In all cases, the errors are several times smaller for HM-FPC than for either HGAM-GS or PACE. In most cases considered here, PACE has larger errors than HGAM-GS, even though this is an ideal case for functional principal components analysis, as the data is generated from model (4) with $K = 2$ functional principal components.

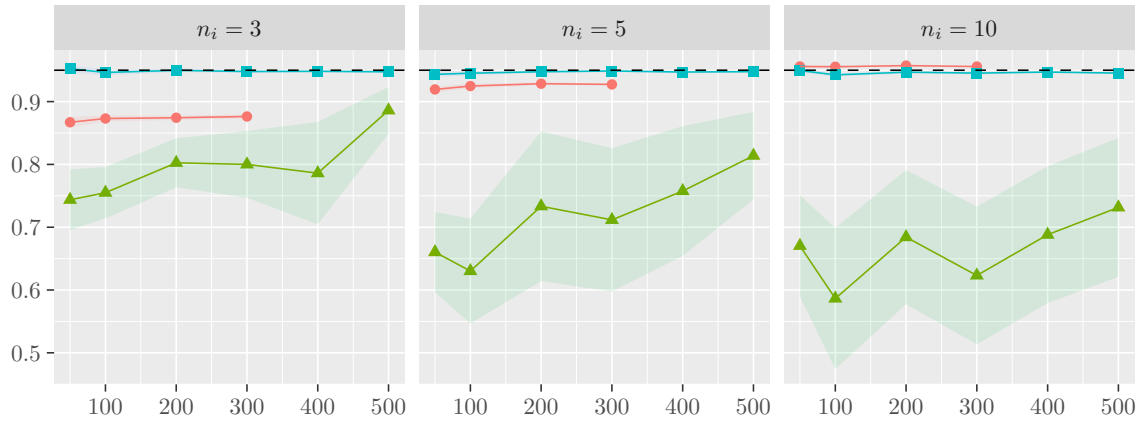
As expected, for all methods the error decreases with the number of observations on each individual n_i . For fixed n_i , the error in HM-FPC initially decreases with d , then stabilises. This is also expected behaviour: we cannot consistently estimate an individual trajectory with only a fixed number of observations on that individual. Instead, for large enough d , HM-FPC and PACE should both behave similarly to an Oracle model, taking (4) with $K = 2$ is known and f_0, f_1, f_2 are fixed at their true values, with only the random effects u_{i1}, u_{i2} unknown. The error in PACE decreases with d , and for larger d than considered here, should eventually converge to the same error as the Oracle model. In practice, it seems that this convergence is very slow, and it would require $d \gg 500$ to match the performance of HM-FPC with $d = 50$.

Figure 3b shows the coverage of nominally 95% confidence intervals. HM-FPC has close to nominal coverage in all cases, whereas HGAM-GS tends to under-cover for small n_i . Figure 3c shows the width of nominally 95% confidence intervals: HM-FPC intervals are far narrower than HGAM-GS intervals. This reinforces the preliminary findings for one simulated dataset with $d = 100$, $n_i = 5$, as shown in Figure 2.

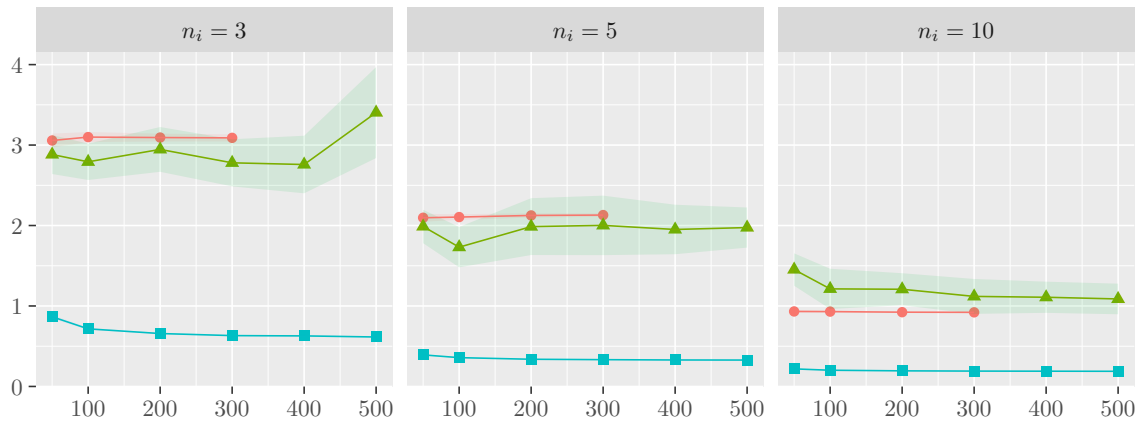
At the population level, Figure 4 gives the root mean 2-Wasserstein error (RMWE) between estimated and true Gaussian processes, and root mean squared errors in the mean function (RMSE_m) and covariance function (RMSE_C). The overall error is far lower for HM-FPC than either HGAM-GS or PACE in all cases, with a particularly large difference when n_i is small. For estimating the mean function, HM-FPC and HGAM-GS have similar errors, while PACE has a larger error. For estimating the covariance function, HM-FPC is far superior to either either HGAM-GS or PACE. HGAM-GS outperforms PACE in most cases considered, except when n_i is small and d is large. HGAM-GS does not give a consistent estimator of the population-level process as d increases,



(a) Root mean integrated squared error

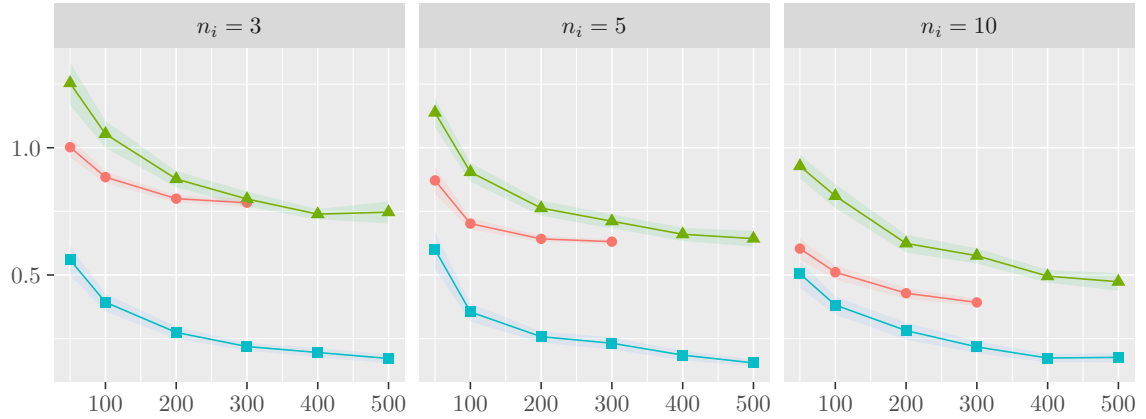


(b) Coverage of confidence intervals (nominal level 0.95)

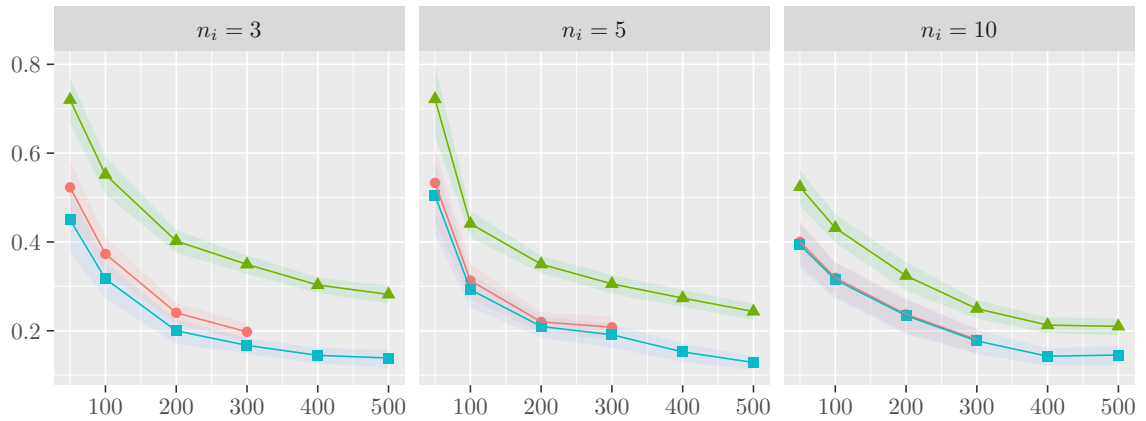


(c) Average width of confidence intervals

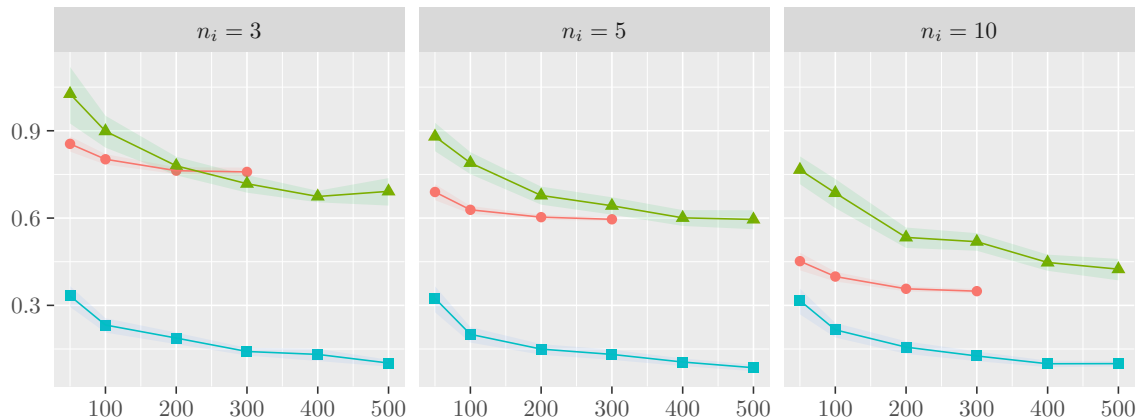
Figure 3: A comparison of methods for inference about the individual trajectories in the 2FPC simulations. The methods shown are HGAM-GS (—●—), PACE (—▲—) and HM-FPC (—■—). Points and shaded bands show estimates and 95% confidence intervals of each quantity based on 100 simulation runs. The plots are split by number of observations per individual, n_i . In each plot, the x -axis is the number of individuals, d . For PACE, the properties of confidence intervals are reported based on the subset of simulation runs for which a confidence interval could be computed (37% of all runs).



(a) Root mean squared 2-Wasserstein error, RMWE



(b) Root mean squared error in the mean, $RMSE_m$



(c) Root mean squared error in the covariance, $RMSE_C$

Figure 4: A comparison of methods for inference about the population-level process in the 2FPC simulations. The methods shown are HGAM-GS (—●—), PACE (—▲—) and HM-FPC (—■—). Points and shaded bands show estimates and 95% confidence intervals of each quantity based on 100 simulation runs. The plots are split by number of observations per individual, n_i . In each plot, the x -axis is the number of individuals, d .

with n_i fixed. HM-FPC and PACE should both give consistent estimators of this population-level process as d grows. As expected, RMWE decreases with d in both cases, though the PACE convergence is slow.

For a typical simulation run with $n_i = 3$ observations on each of $d = 300$ individuals, Figure 5 shows a range of estimated individual trajectories. HM-FPC gives by far the most accurate estimates of the trajectories, with narrow confidence intervals even for regions far from the data. Figure 6 shows the estimated population mean, variance and correlation functions for each method, for the same typical simulation run. All methods do reasonably well capturing the shape of the population mean, though PACE has higher error than other methods. HM-FPC gives the best estimate of the variance, and is the only method able to accurately capture the correlation structure.

4.5.2 LMM-RI

We simulate data from a random intercept model

$$y_{ij} = \beta_0 + \beta_1 t_{ij} + u_{0i} + \epsilon_{ij}, \quad i = 1, \dots, d, \quad j = 1, \dots, n_i,$$

where $u_{0i} \sim N(0, \sigma_u^2)$ and $\epsilon_{ij} \sim N(0, \sigma^2)$. We generate data with parameter values $\beta_0 = -1$, $\beta_1 = 2$, $\sigma_u = 0.5$, $\sigma = 0.1$. The time points t_{ij} are uniformly distributed on $[0, 1]$. For comparison, in addition to the common set of fitting methods from section 4.3, we also fit a linear mixed model with random intercepts (LMM-RI).

A full description of the results in this case is given in Appendix B. In summary, estimated trajectories from HGAM-GS, HM-FPC and LMM-RI all behave similarly, while PACE has errors several times larger than the other methods. HM-FPC and HGAM-GS provide confidence intervals with close to nominal coverage in all cases, whereas PACE under-covers.

4.5.3 SITAR

SITAR (Cole et al., 2010) is often used for modelling height growth curves. It is a non-linear random effects model, in which

$$\mu_i(t) = \alpha_i + h \left(\frac{t - \beta_i}{\exp(-\gamma_i)} \right), \quad (22)$$

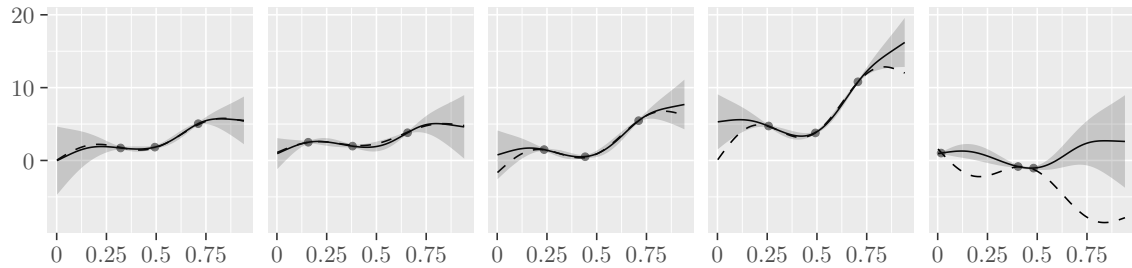
where $\alpha_i, \beta_i, \gamma_i$ are random effects, and $h(\cdot)$ is an unknown function which must be estimated. The R package `sitar` (Cole, 2023) may be used to fit this model.

In order to simulate data from a realistic process, we first fit a SITAR model to some real heights, then simulate data from the fitted model. The data we use is on heights of girls aged 8–18, from the Berkeley Child Guidance Study dataset (Tuddenham and Snyder, 1954). The data is available as `berkeley` in the `sitar` R package, and the subset of the data we use here is also used in the package `vignette`. SITAR appears to provide a good fit to this data. There are other cases for which SITAR performs less well, such as modelling heights over the whole of childhood (e.g. girls aged 0–18 in the `berkeley` data).

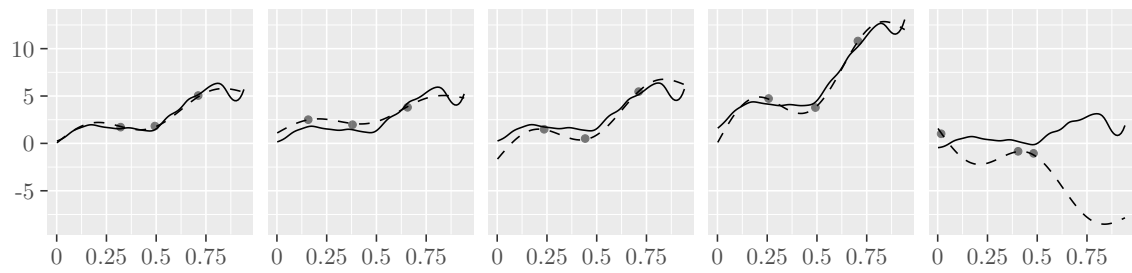
Having fit a SITAR model, we then simulate new data from the fitted model. We generate data from 18 processes of this form, given by all possible combinations of $d \in \{50, 100, 200, 300, 400, 500\}$ and $n_i \in \{3, 5, 10\}$. For each individual, the first observation time t_{i1} is uniformly distributed on $[8, 8 + h]$, where $h = (18 - 8)/n_i$, with the remaining heights $t_{ij} = t_{i1} + (j - 1)h$ spaced h years apart. For comparison, in addition to the methods described in section 4.3, we also fit the true SITAR model.

In this case, the model (4) is not correct. This data generating process cannot be expressed in terms of any finite number of functional principal components, and in the infinite Karhunen-Lo  ve decomposition (2), the coefficients u_{ki} are not normally distributed. However, there are strong structural similarities between individual trajectories, and the first three functional principal components explain 99.7% of the variation between the individual trajectories.

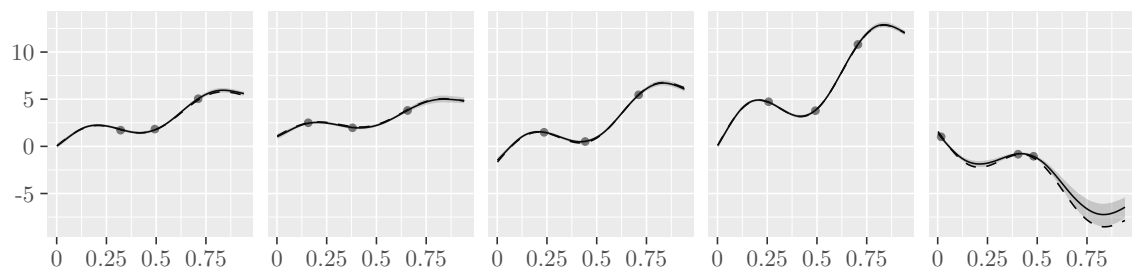
A full description of the results in this case is given in Appendix C. In summary, HM-FPC substantially outperforms PACE in all cases, and HGAM-GS in all cases with $n_i \leq 5$. For $n_i = 10$,



(a) HGAM-GS



(b) PACE



(c) HM-FPC

Figure 5: Fitted trajectories with 95% pointwise confidence intervals, for four individuals in a typical run (seed = 22) of the 2FPC simulations, with $d = 300$ individuals and $n_i = 3$ observations on each individual. The individuals are selected to show a range of combined errors, from least error on the left to most error on the right. Fitted trajectories are shown as solid lines, confidence intervals (where available) as shaded regions and data as points. The true trajectories used to generate the data are overlaid as dashed lines.

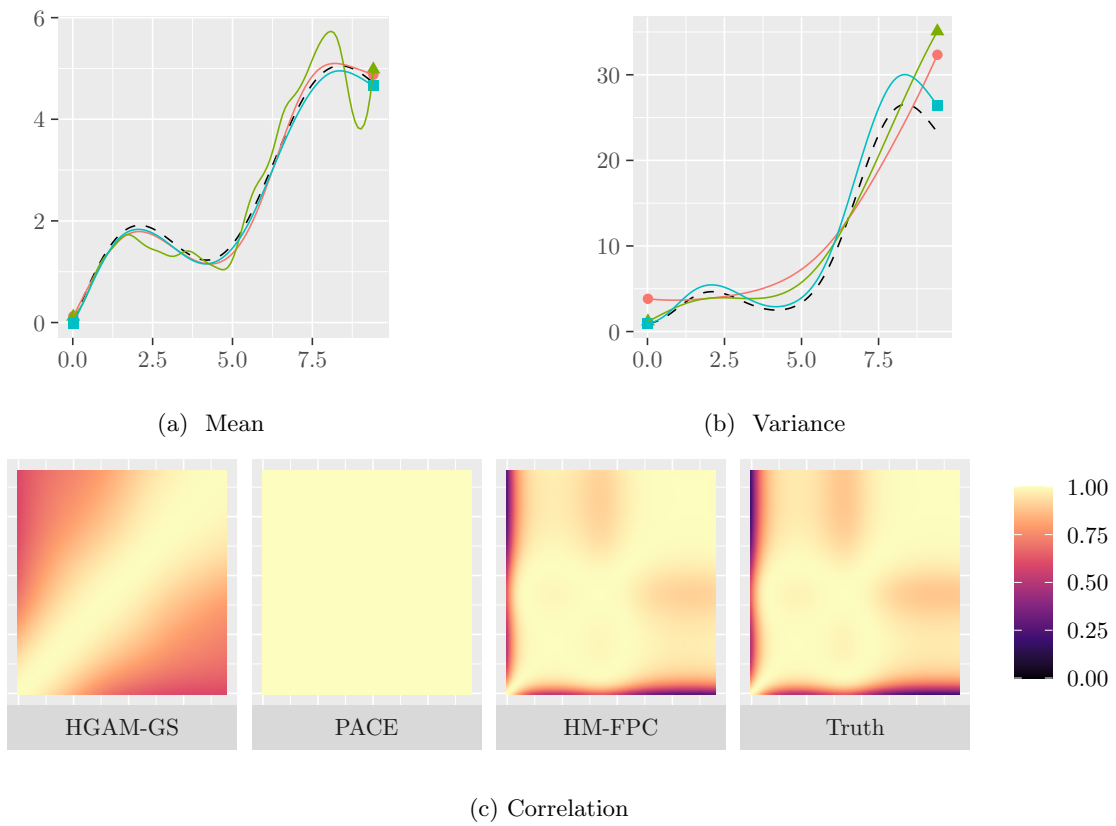


Figure 6: A comparison of population mean, variance and correlation functions for a typical run (seed = 47) of the 2FPC simulations, with $d = 300$ individuals and $n_i = 3$ observations on each individual. In a and b, the methods shown are HGAM-GS (—●—), PACE (—▲—) and HM-FPC (—■—), with the truth overlaid as a dashed curve.

HM-FPC and HGAM-GS perform similarly. As expected, SITAR is the best performing method in most cases, though model fitting fails or gives very large errors in all cases with $n_i = 3$ and with $n_i = 5, d \leq 100$. In that challenging very sparse setup, HM-FPC substantially outperforms all other methods, even though the model (4) is not correct.

5 Application: percent body fat in adolescent girls

We consider data on body fat measurements taken from the MIT Growth and Development Study, originally studied by Phillips et al. (2003). The data is used as an example in Fitzmaurice et al. (2011), and is made available as the `fat` data in the associated ALA R package (Luque and Bates, 2012). The `fat` data is provided by the ALA R package, subject to the note that the data “represent a subset of the study materials and should not be used to draw substantive conclusions”. We use this data to demonstrate methodology, and the conclusions we make should not be treated as substantive scientific conclusions.

The data contains measurements of percent body fat for 162 girls, in the years before and after menarche (time of first period). Measurements were taken roughly annually, with the last appointment scheduled four years after menarche. Time is rescaled to be relative to time of menarche, so that zero represents reported time of menarche. The number of observations on each subject ranges from 3 and 10, with a mean of 6.5.

Preliminary analysis reveals that percentage fat tends to increase over time, but this increase does not appear to be linear. Fitzmaurice et al. (2011) show that on average, percent body fat seems to increase more slowly before menarche than after.

We fit a hierarchical model with functional principal components to this data. We choose $K = 4$ components, and estimate the error standard deviation as $\hat{\sigma} = 0.32$.

Figure 7 shows estimated percent body fat $\hat{\mu}_i(t)$ for the first twenty girls, with 95% confidence intervals. The fit appears reasonable, but some work is needed to generalise beyond individuals, to understand how percent fat body varies with time in the population as whole.

Figure 8 shows estimates and confidence interval for the population averaged mean curve. The population averaged mean curve from the piecewise linear model from Fitzmaurice et al. (2011) is overlaid. From this, it is clear that there is variation in the population averaged percent fat beyond this piecewise linear model. On average, there is relatively little change in percent body fat until around 6 months before menarche. From there until around 2 years after menarche there is a rapid increase in average percent body fat. From 2 to 4 years after menarche, percent body fat is still increasing on average, but at a slower rate.

The population averaged percent body fat is not informative about variation between subjects. We might be interested in such variation, as well as the average behaviour. Figure 9 summarises the diversity of estimated rates of fat growth between different subjects, showing the median estimated rate of fat growth, and bands covering the central 50% and 90% of subjects.

Nearly all subjects are estimated to have increasing percent body fat from shortly before menarche until 2 years after, with rapid growth (at least 2 percentage points per year) around 6 months after menarche. There is far more diversity among subjects before menarche, with three quarters of subjects estimated to have decreasing body fat around 2 years before menarche.

6 Discussion and Future Work

The setup of this paper was simple: modelling how individual responses vary with time, without additional explanatory variables. Despite the simplicity of the setup, all existing methods considered failed in some of the cases we studied. Simple mixed-effects models make strong assumptions about the relationship between the subject-specific mean curves (e.g. that they vary only in intercept or slope), while existing hierarchical generalised additive models fail to exploit structural similarities in the individual trajectories. Functional principal components analysis allows for general relationships between the curves, but existing methods, such as PACE, did not work well in many of our simulated examples, particularly in cases with a small number of observations on each subject. Our new hierarchical modelling with functional principal components approach

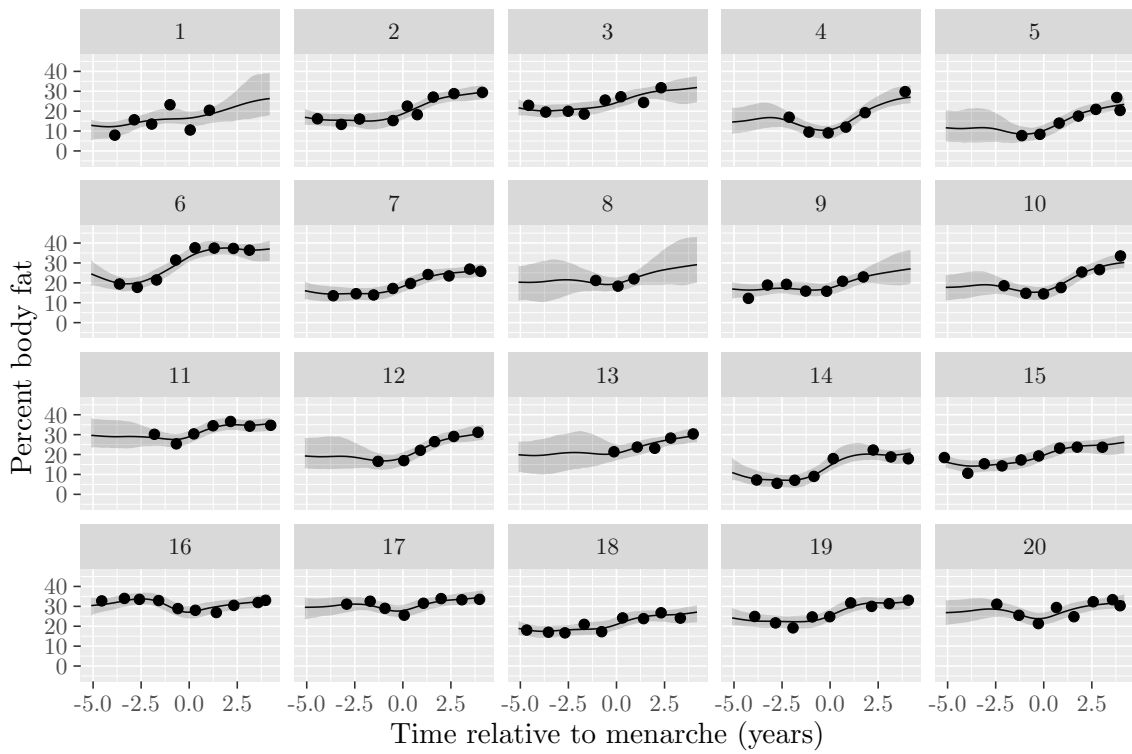


Figure 7: Percentage body fat against time, for the first twenty girls in the `fat` data, with fitted curves and 95% confidence intervals overlaid.

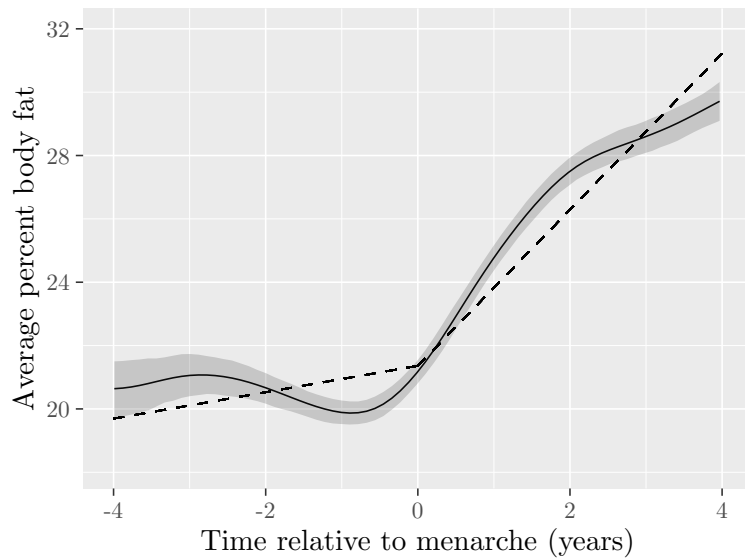


Figure 8: The population-averaged percent body fat over time, with 95% confidence intervals. The dashed line is the estimated population-averaged curve using the piecewise linear model from Fitzmaurice et al. (2011).

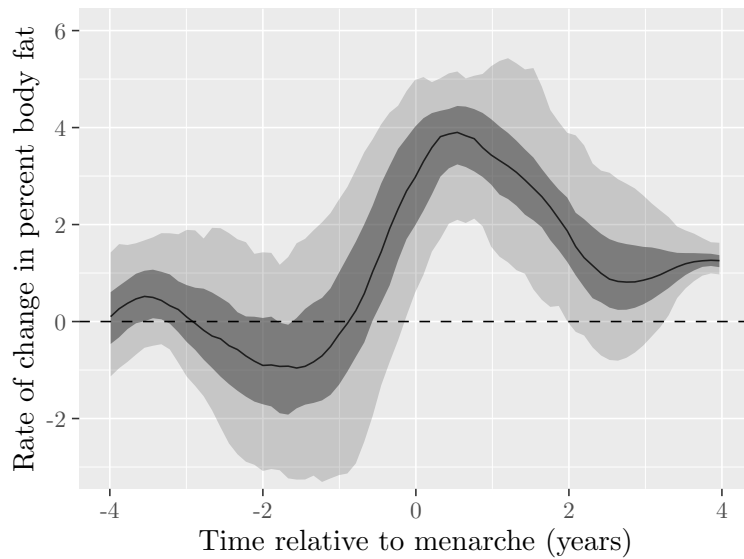


Figure 9: The distribution of the estimated rate of change in percent body fat across subjects. The solid line shows the median, the darker shaded region is 25th to 75th quantile, the lighter shaded region is 5th to 95th quantile.

offers much improved inference, and fulfils the promise of FPCA to exploit structural similarities in trajectories.

Future work will focus on extensions to make the methodology more widely applicable, by allowing for dependence on additional explanatory variables in the model, and generalising to different types of response distribution (for instance to allow for binary or count data).

This paper described models for longitudinal data, but all of these models may also be used for clustered data, with clusters i , and any continuous explanatory variable in place of time t . Mixed-effects models are also used for more complex clustered data, such as multiple nested levels of clustering. Another avenue for future work is to consider the extension of these models to allow for more complex clustering.

Code availability

The new hierarchical modelling with functional principal components method is implemented in R package `flexl`, available at <https://github.com/heogden/flexl>

Acknowledgements

The author acknowledges the use of the IRIDIS High Performance Computing Facility, and associated support services at the University of Southampton, in the completion of this work.

References

- T. Cole. *sitar: Super Imposition by Translation and Rotation Growth Curve Analysis*, 2023. URL <https://CRAN.R-project.org/package=sitar>. R package version 1.4.0.
- T. J. Cole, M. D. C. Donaldson, and Y. Ben-Shlomo. SITAR – a useful instrument for growth curve analysis. *International Journal of Epidemiology*, 39(6):1558–1566, 2010.

- C.-Z. Di, C. M. Crainiceanu, B. S. Caffo, and N. M. Punjabi. Multilevel functional principal component analysis. *The Annals of Applied Statistics*, 3(1):458 – 488, 2009. doi: 10.1214/08-AOAS206.
- A. Elhakeem, R. A. Hughes, K. Tilling, D. L. Cousminer, S. A. Jackowski, T. J. Cole, A. S. F. Kwong, Z. Li, S. F. A. Grant, A. D. G. Baxter-Jones, B. S. Zemel, and D. A. Lawlor. Using linear and natural cubic splines, sitar, and latent trajectory models to characterise nonlinear longitudinal growth trajectories in cohort studies. *BMC Medical Research Methodology*, 22(1): 68, 2022.
- G. M. Fitzmaurice, N. M. Laird, and J. H. Ware. *Applied Longitudinal Analysis*. John Wiley & Sons, second edition, 2011. doi: 10.1002/9781119513469.
- J. Goldsmith, S. Greven, and C. Crainiceanu. Corrected confidence bands for functional data using principal components. *Biometrics*, 69(1):41–51, 2013. doi: 10.1111/j.1541-0420.2012.01808.x.
- J. Goldsmith, F. Scheipl, L. Huang, J. Wrobel, C. Di, J. Gellar, J. Harezlak, M. W. McLean, B. Swihart, L. Xiao, C. Crainiceanu, and P. T. Reiss. *refund: Regression with Functional Data*, 2023. URL <https://CRAN.R-project.org/package=refund>. R package version 0.1-30.
- X. Lin and D. Zhang. Inference in generalized additive mixed models by using smoothing splines. *Journal of the Royal Statistical Society Series B: Statistical Methodology*, 61(2):381–400, 1999.
- S. P. Luque and D. Bates. *ALA: Data sets and examples for the book “Applied Longitudinal Analysis”*, 2012. URL <https://R-Forge.R-project.org/projects/applong/>. R package version 1.0/r53.
- I. Olkin and F. Pukelsheim. The distance between two random vectors with given dispersion matrices. *Linear Algebra and its Applications*, 48:257–263, 1982. doi: 10.1016/0024-3795(82)90112-4.
- E. J. Pedersen, D. L. Miller, G. L. Simpson, and N. Ross. Hierarchical generalized additive models in ecology: an introduction with mgcv. *PeerJ*, 7:e6876, 2019.
- S. M. Phillips, L. G. Bandini, D. V. Compton, E. N. Naumova, and A. Must. A longitudinal comparison of body composition by total body water and bioelectrical impedance in adolescent girls. *The Journal of Nutrition*, 133(5):1419–1425, 2003. doi: 10.1093/jn/133.5.1419.
- A. Redd. *orthogonalsplinebasis: Orthogonal B-Spline Basis Functions*, 2022. URL <https://CRAN.R-project.org/package=orthogonalsplinebasis>. R package version 0.1.7.
- Stan Development Team. StanHeaders: Headers for the R interface to Stan, 2020. URL <https://mc-stan.org/>. R package version 2.21.0-6.
- R. D. Tuddenham and M. M. Snyder. Physical growth of California boys and girls from birth to eighteen years. *University of California publications in child development*, 1(2), 1954.
- S. N. Wood. *Generalized Additive Models: An Introduction with R*. Chapman and Hall/CRC, second edition, 2017.
- F. Yao, H.-G. Müller, and J.-L. Wang. Functional data analysis for sparse longitudinal data. *Journal of the American Statistical Association*, 100(470):577–590, 2005. doi: 10.1198/016214504000001745.
- Y. Zhou, S. Bhattacharjee, C. Carroll, Y. Chen, X. Dai, J. Fan, A. Gajardo, P. Z. Hadjipantelis, K. Han, H. Ji, C. Zhu, H.-G. Müller, and J.-L. Wang. *fdapace: Functional Data Analysis and Empirical Dynamics*, 2022. URL <https://CRAN.R-project.org/package=fdapace>. R package version 0.5.9.

A Proofs

Proof of Claim 1. By differentiating (4) twice, we have

$$\mu_i''(t) = f_0''(t) + \sum_{k=1}^K u_{ik} f_k''(t),$$

so

$$[\mu_i''(t)]^2 = (f_0''(t))^2 + 2f_0''(t) \sum_{k=1}^K u_{ik} f_k''(t) + \sum_{k=1}^K \sum_{l=1}^K u_{ik} u_{il} f_k''(t) f_l''(t).$$

So

$$w(\mu_i) = w(f_0) + 2 \sum_{k=1}^K u_{ik} \int_{-\infty}^{\infty} f_0''(t) f_k''(t) dt + \sum_{k=1}^K \sum_{l=1}^K u_{ik} u_{il} \int_{-\infty}^{\infty} f_k''(t) f_l''(t) dt$$

and

$$\begin{aligned} w_E &= E[w(\mu_i)] \\ &= w(f_0) + 2 \sum_{k=1}^K E(u_{ik}) \int_{-\infty}^{\infty} f_0''(t) f_k''(t) dt + \sum_{k=1}^K \sum_{l=1}^K E(u_{ik} u_{il}) \int_{-\infty}^{\infty} f_k''(t) f_l''(t) dt \\ &= w(f_0) + \sum_{k=1}^K E(u_{ik}^2) \int_{-\infty}^{\infty} (f_k''(t))^2 dt \end{aligned}$$

since u_{ik} are independent, with mean zero

$$= w(f_0) + \sum_{k=1}^K w(f_k),$$

since $E(u_{ik}^2) = \text{Var}(u_{ik}) = 1$, as required. □

Proof of Claim 2. For any i and j , we have

$$\begin{aligned} \langle f_i, f_j \rangle &= \left\langle \sum_{k=1}^{n_B} \beta_{ik} b_k, \sum_{l=1}^{n_B} \beta_{jl} b_l \right\rangle \\ &= \sum_{k=1}^{n_B} \sum_{l=1}^{n_B} \beta_{ik} \beta_{jl} \langle b_k, b_l \rangle \\ &= \sum_{l=1}^{n_B} \beta_{il} \beta_{jl} = \langle \beta_i, \beta_j \rangle \end{aligned}$$

since $\langle b_k, b_l \rangle = 0$ if $k \neq l$ and $\langle b_l, b_l \rangle = 1$.

So $\langle f_i, f_j \rangle = 0$ if and only if $\langle \beta_i, \beta_j \rangle = 0$, and the result follows. □

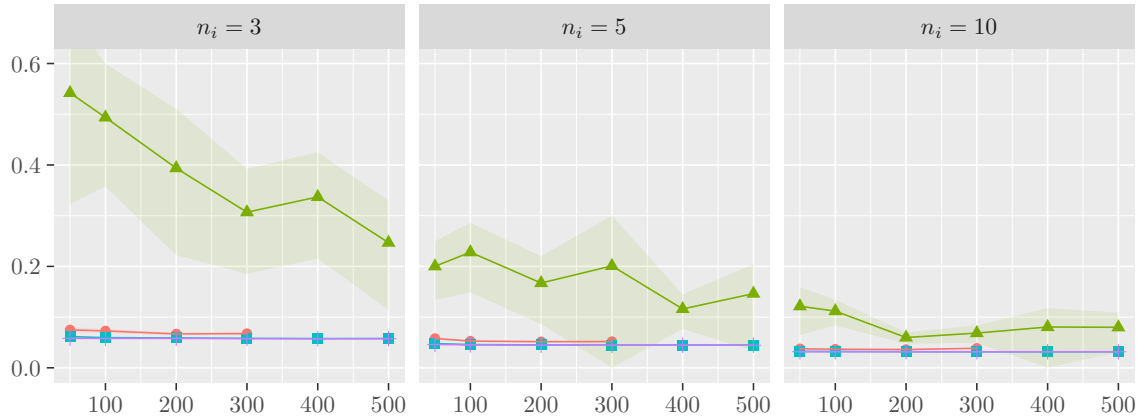
B Detailed results of LMM-RI simulations

Figure 10a shows the RMISE for each choice of number of individual d and number of observations on each individual n_i . In all cases, HGAM-GS, HM-FPC and LMM-RI behave similarly, while PACE has errors several times larger than the other methods.

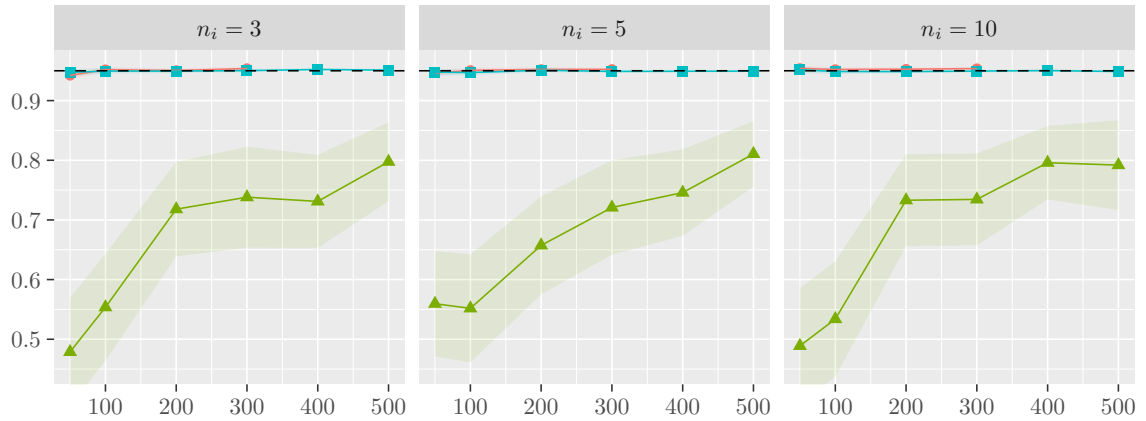
Figure 10b shows the coverage of nominally 95% confidence intervals. HM-FPC and HGAM-GS have close to nominal coverage in all cases, whereas PACE under-covers.

At the population level, Figure 11 gives the root mean 2-Wasserstein error between estimated and true Gaussian processes generating the trajectories. Again, PACE is outperformed by all other methods, although all methods estimate the population-level processes well.

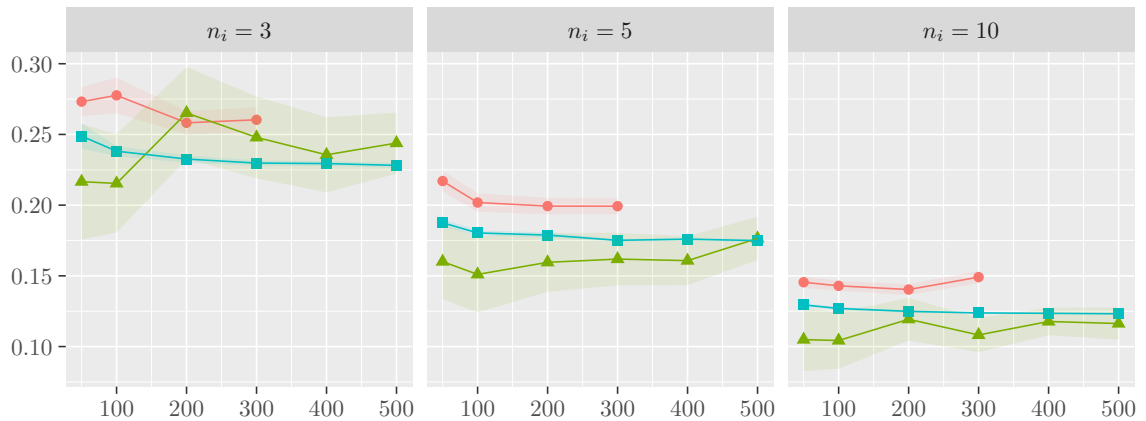
For a typical simulation run with $n_i = 3$ observations on each of $d = 300$ individuals, Figure 12 shows a range of estimated individual trajectories. All methods estimate the trajectories well in most cases, but PACE performs poorly in the challenging case on the right, for which observations are only available at one end of the time interval. Figure 13 shows the estimated population mean, variance and correlation functions for each method, for the same typical simulation run. HM-FPC provides high-quality estimates of all quantities. HGAM-GS estimates the mean and correlation structure well, but provides a less good estimate of the variance. PACE performs worse than the other methods in this case, with a worse estimate of the correlation structure.



(a) Root mean integrated squared error

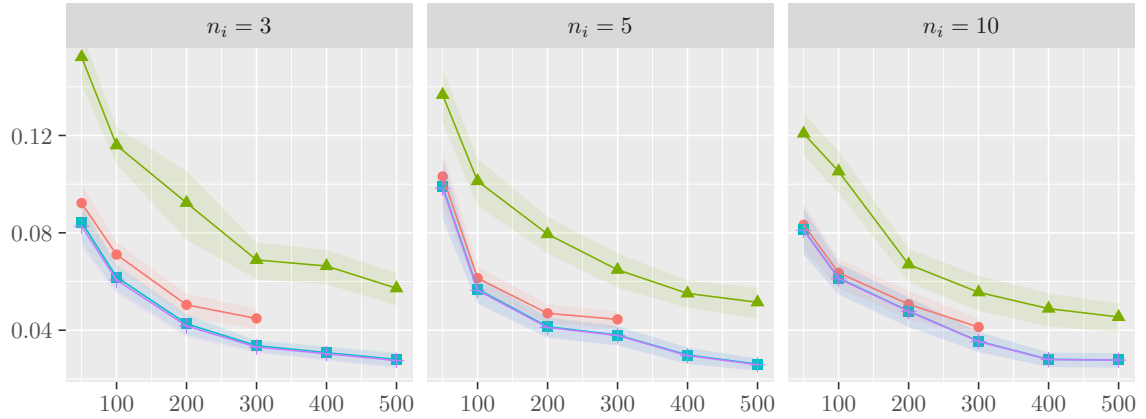


(b) Coverage of confidence intervals (nominal level 0.95)

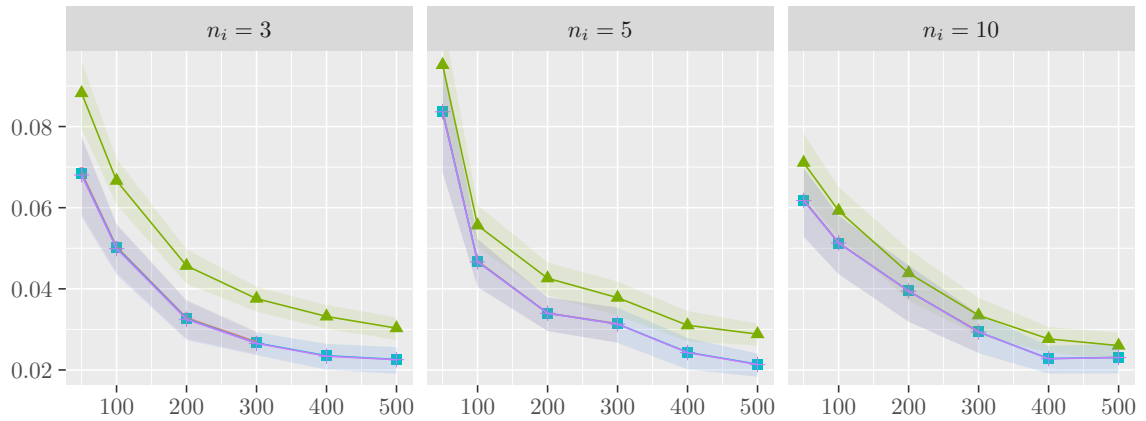


(c) Average width of confidence intervals

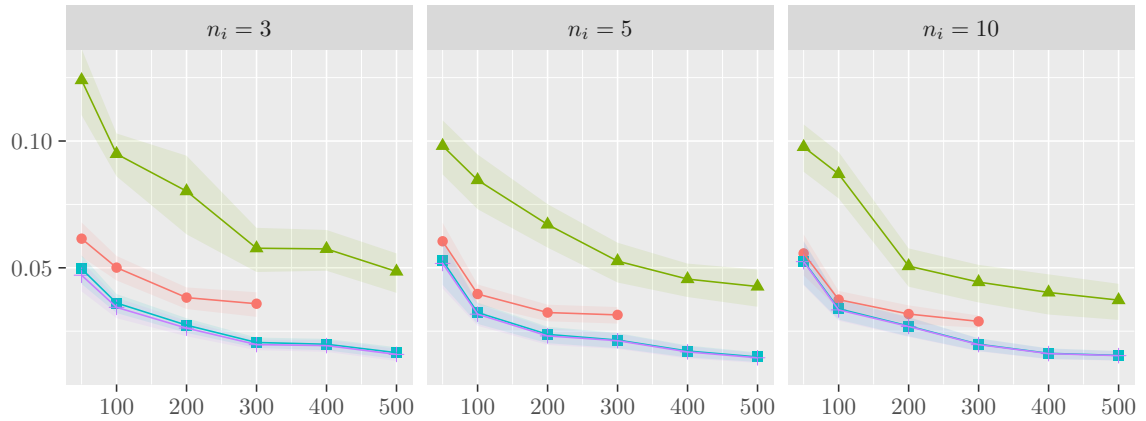
Figure 10: A comparison of methods for inference about the individual trajectories in the LMM-RI simulations. The methods shown are HGAM-GS (—●—), PACE (—▲—), HM-FPC (—■—) and LMM-RI (—+—). Points and shaded bands show estimates and 95% confidence intervals of each quantity based on 100 simulation runs. The plots are split by number of observations per individual, n_i . In each plot, the x -axis is the number of individuals, d . For PACE, the properties of confidence intervals are reported based on the subset of simulation runs for which a confidence interval could be computed (74% of all runs).



(a) Root mean squared 2-Wasserstein error, RMWE

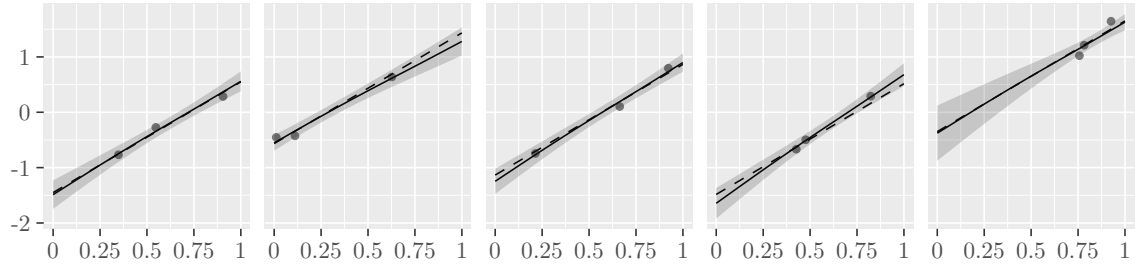


(b) Root mean squared error in the mean, $RMSE_m$

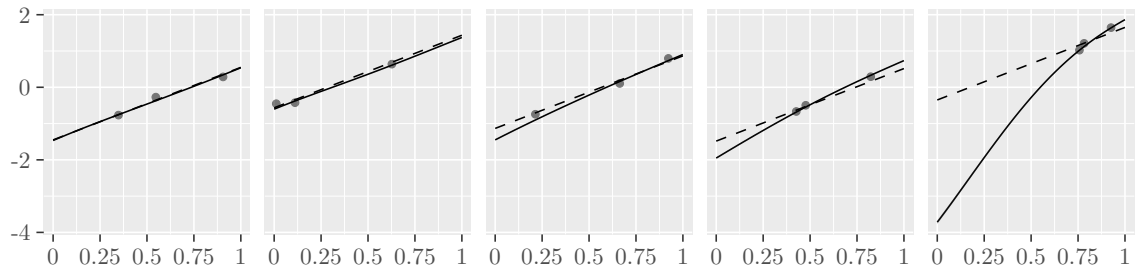


(c) Root mean squared error in the covariance, $RMSE_C$

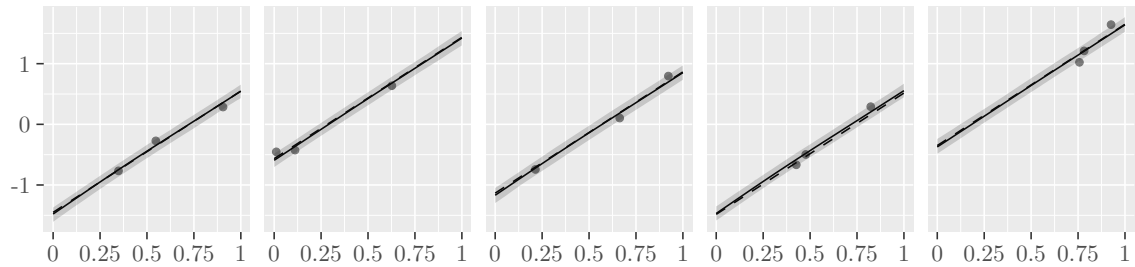
Figure 11: A comparison of methods for inference about the population-level process in the LMM-RI simulations. The methods shown are HGAM-GS (—●—), PACE (—▲—), HM-FPC (—■—) and LMM-RI (—+—). Points and shaded bands show estimates and 95% confidence intervals of each quantity based on 100 simulation runs. The plots are split by number of observations per individual, n_i . In each plot, the x -axis is the number of individuals, d .



(a) HGAM-GS



(b) PACE



(c) HM-FPC

Figure 12: Fitted trajectories with 95% pointwise confidence intervals, for four individuals in a typical run (seed = 22) of the LMM-RI simulations, with $d = 300$ individuals and $n_i = 3$ observations on each individual. The individuals are selected to show a range of combined errors, from least error on the left to most error on the right. Fitted trajectories are shown as solid lines, confidence intervals (where available) as shaded regions and data as points. The true trajectories used to generate the data are overlaid as dashed lines.

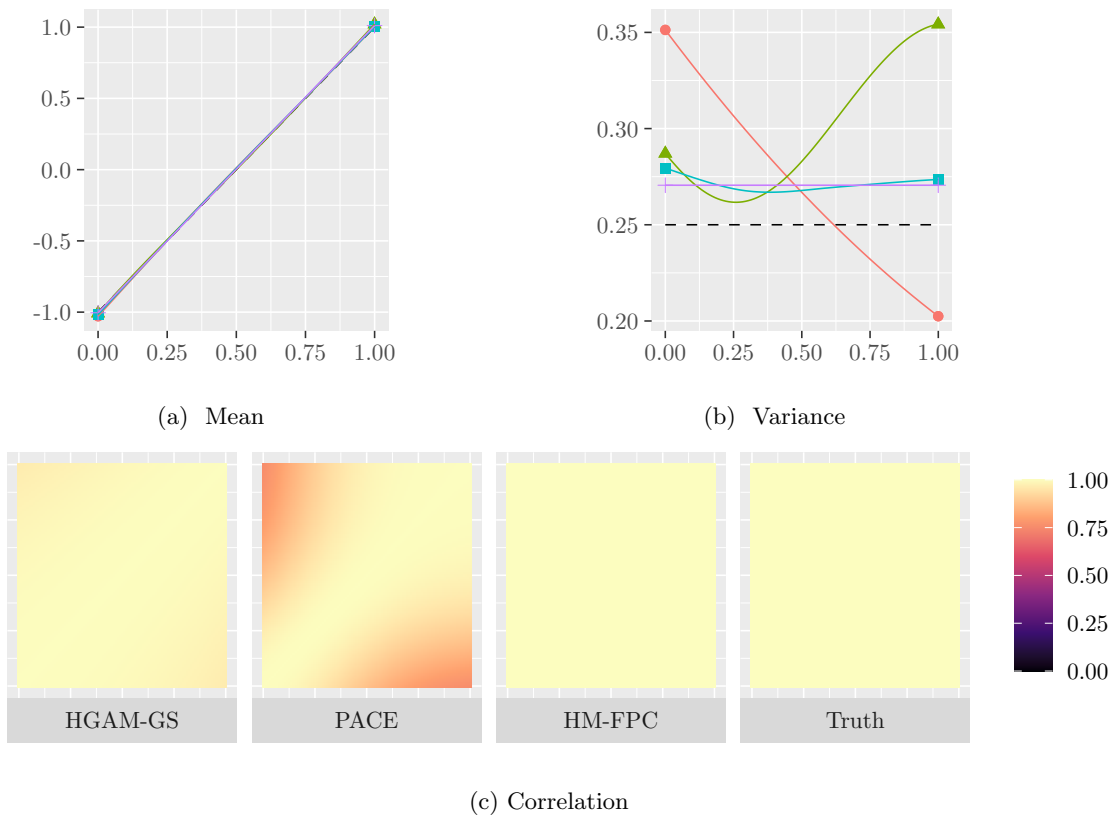


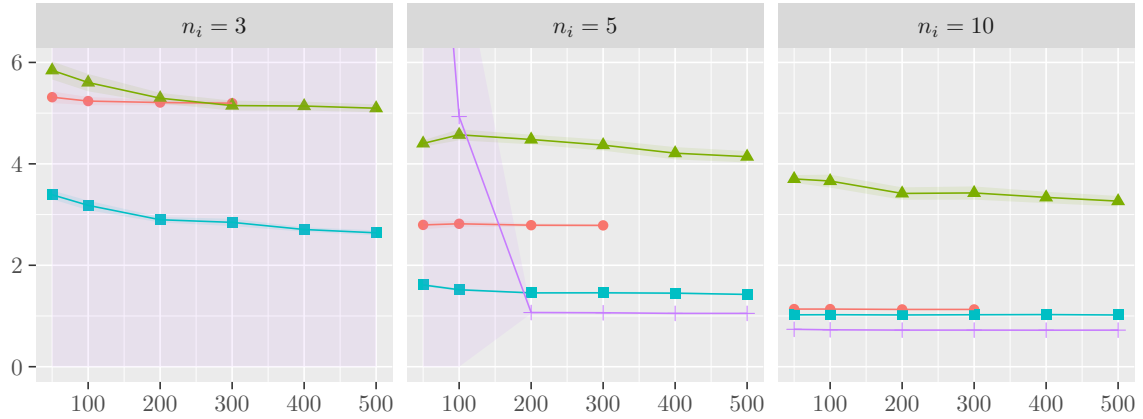
Figure 13: A comparison of population mean, variance and correlation functions for a typical run (seed = 22) of the LMM-RI simulations, with $d = 300$ individuals and $n_i = 3$ observations on each individual. In a and b, the methods shown are HGAM-GS (—●—), PACE (—▲—), HM-FPC (—■—), and LMM-RI (—+—), with the truth overlaid as a dashed curve.

C Detailed results of SITAR simulations

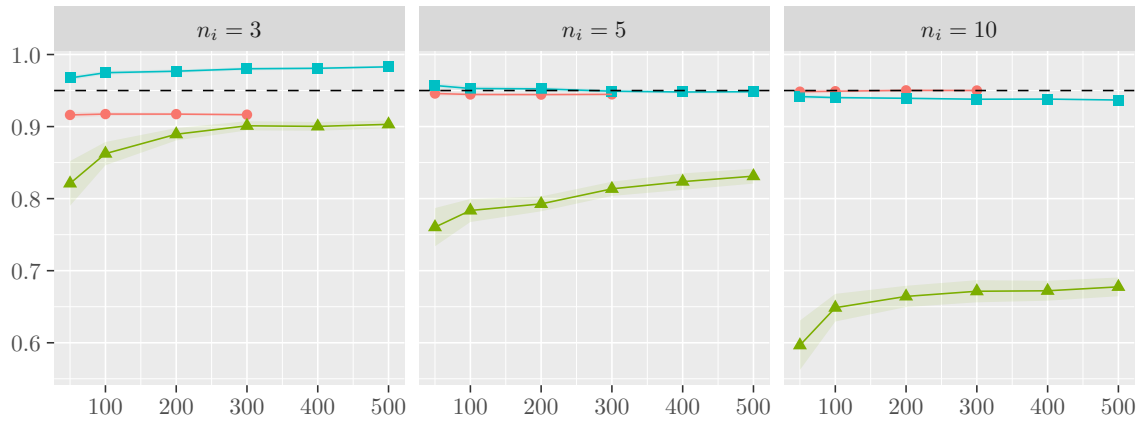
Figure 14a shows the RMISE for each choice of number of individual d and number of observations on each individual n_i . HM-FPC has substantially lower errors than PACE in all cases, and also outperforms HGAM-GS in all cases with $n_i \leq 5$. For $n_i = 10$, PACE and HGAM-GS perform similarly. As expected, SITAR has the lowest errors in most cases, though model fitting fails or gives very large errors in all cases with $n_i = 3$ and with $n_i = 5, d \leq 100$.

Figure 14b shows the coverage of nominally 95% confidence intervals, and Figure 14c shows the average widths of those intervals. Intervals from SITAR were not easily available in the `sitar` R package, so are not included in the comparison. For PACE, confidence intervals could be computed in nearly all simulation runs (only one run gave an error), by contrast with the 2FPC and LMM-RI cases. The HM-FPC intervals are the shortest, and have close to nominal coverage, though they slightly under-cover for $n_i = 10$. PACE under-covers in all cases, and HGAM-GS under-covers for $n_i = 3$.

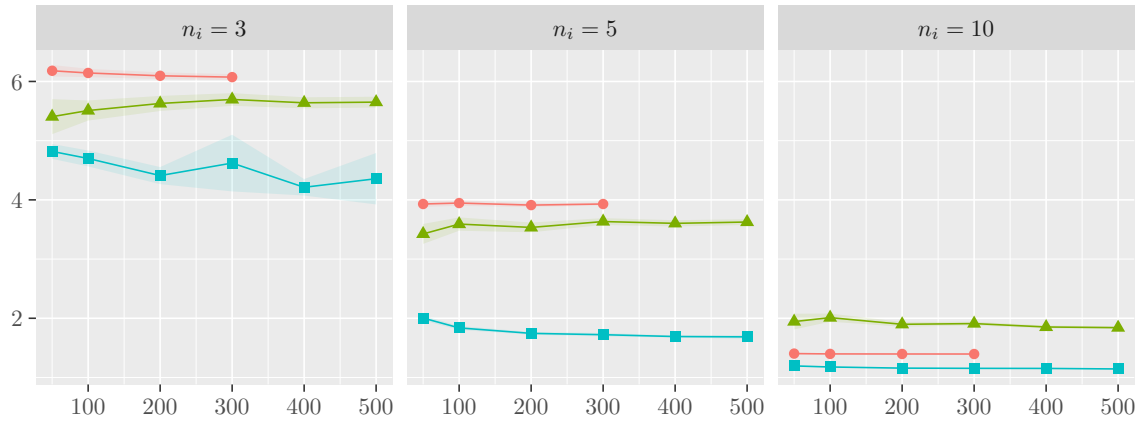
For a typical simulation run with $n_i = 5$ observations on each of $d = 300$ individuals, Figure 16 shows a range of estimated individual trajectories. All methods provide reasonable estimates of the individual trajectories, but the HM-FPC estimates are superior for the more challenging cases (towards the right), and HM-FPC has noticeably narrower confidence intervals than other methods. None of these methods includes any monotonicity constraint, and in the case on the right, all the estimated trajectories are decreasing in some time intervals. One avenue for future work could be to allow a monotonicity constraint to be enforced in the HM-FPC framework. Figure 17 shows the estimated population mean, variance and correlation functions for each method, for the same typical simulation run. All methods provide excellent estimates of the population mean. HM-FPC gives by far the best estimate of the variance and correlation structure.



(a) Root mean integrated squared error

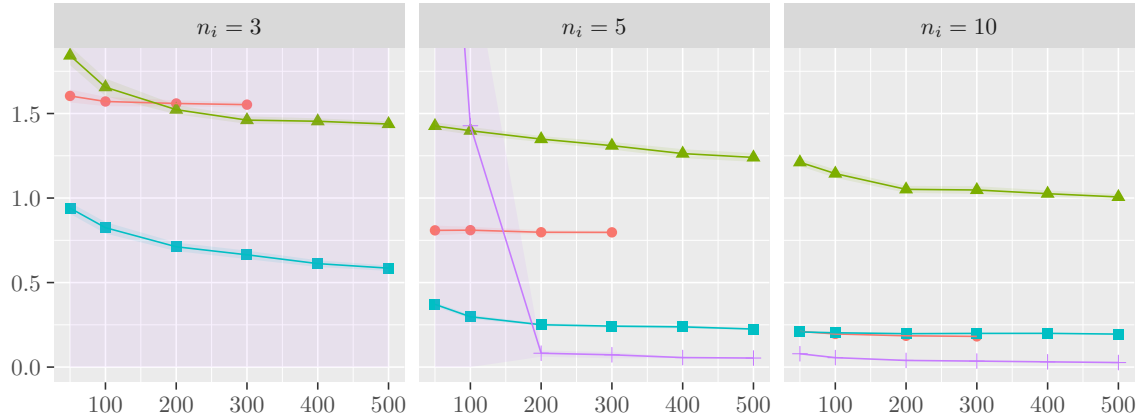


(b) Coverage of confidence intervals (nominal level 0.95)

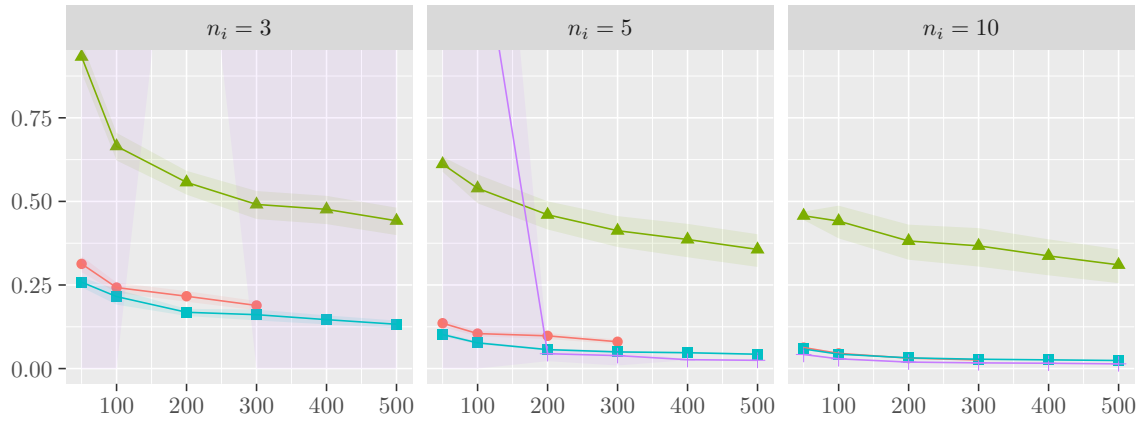


(c) Average width of confidence intervals

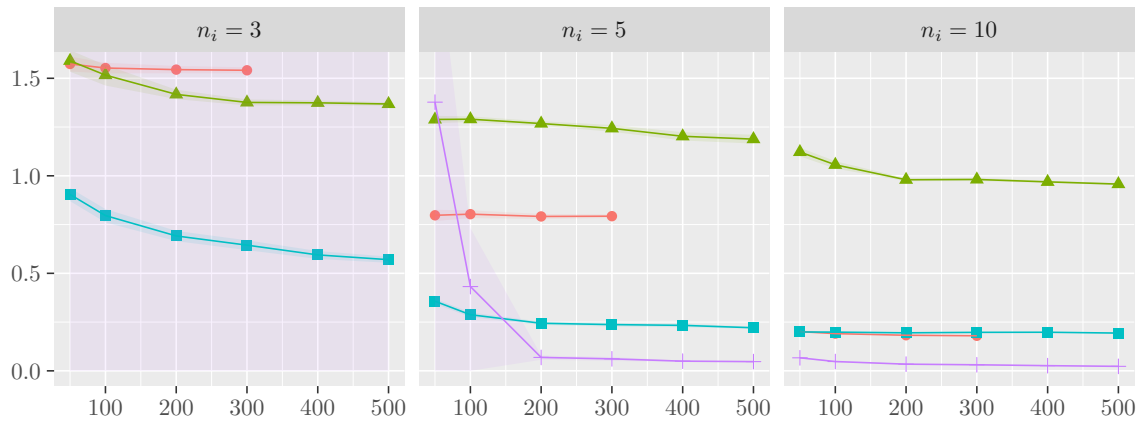
Figure 14: A comparison of methods for inference about the individual trajectories in the SITAR simulations. The methods shown are HGAM-GS (—●—), PACE (—▲—), HM-FPC (—■—) and SITAR (—+—). Points and shaded bands show estimates and 95% confidence intervals of each quantity based on 100 simulation runs. The plots are split by number of observations per individual, n_i . In each plot, the x -axis is the number of individuals, d .



(a) Root mean squared 2-Wasserstein error, RMWE, relative to a Gaussian process with the true mean and covariance functions.

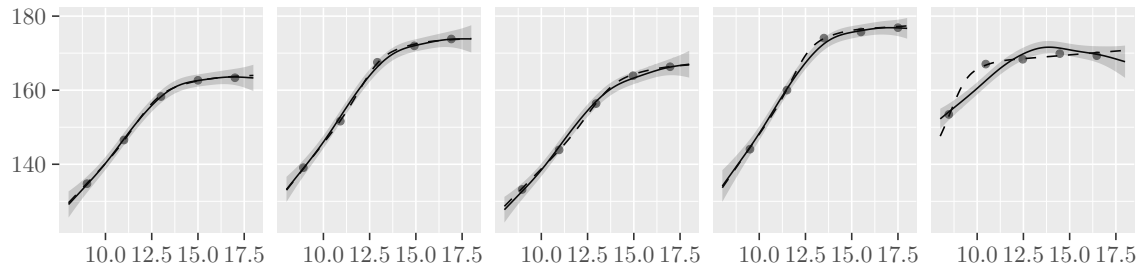


(b) Root mean squared error in the mean, $RMSE_m$

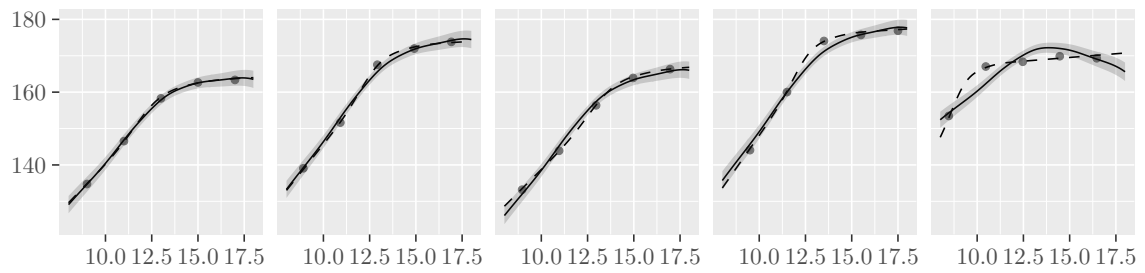


(c) Root mean squared error in the covariance, $RMSE_C$

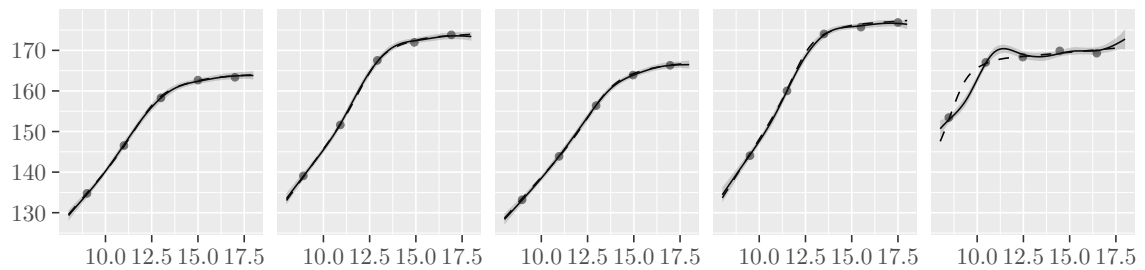
Figure 15: A comparison of methods for inference about the population-level process in the SITAR simulations. The methods shown are HGAM-GS (—●—), PACE (—▲—), HM-FPC (—■—) and SITAR (—+—). Points and shaded bands show estimates and 95% confidence intervals of each quantity based on 100 simulation runs. The plots are split by number of observations per individual, n_i . In each plot, the x -axis is the number of individuals, d .



(a) HGAM-GS



(b) PACE



(c) HM-FPC

Figure 16: Fitted trajectories with 95% pointwise confidence intervals, for four individuals in a typical run (seed = 54) of the SITAR simulations, with $d = 300$ individuals and $n_i = 5$ observations on each individual. The individuals are selected to show a range of combined errors, from least error on the left to most error on the right. Fitted trajectories are shown as solid lines, confidence intervals (where available) as shaded regions and data as points. The true trajectories used to generate the data are overlaid as dashed lines.

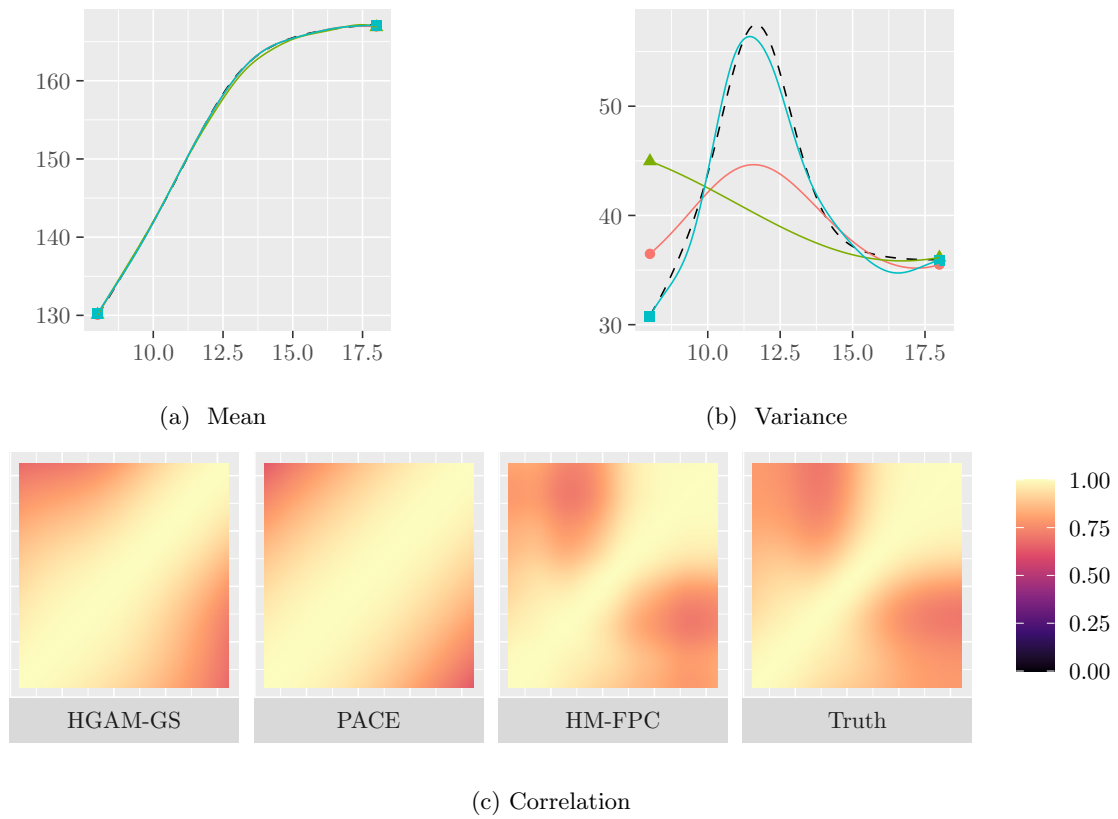


Figure 17: A comparison of population mean, variance and correlation functions for a typical run (seed = 54) of the SITAR simulations, with $d = 300$ individuals and $n_i = 5$ observations on each individual. In a and b, the methods shown are HGAM-GS (—●—), PACE (—▲—) and HM-FPC (—■—), with the truth overlaid as a dashed curve.